

Progressive meristem and single-cell transcriptomes reveal the regulatory mechanisms underlying maize inflorescence development and sex differentiation

Yonghao Sun^{1,2,5}, Liang Dong^{1,5}, Lu Kang^{1,5}, Wanshun Zhong¹, David Jackson^{1,3} and Fang Yang^{1,4,*}

¹National Key Laboratory of Crop Genetic Improvement, Huazhong Agricultural University, Wuhan 430070, China

²Hubei Hongshan Laboratory, Wuhan 430070, China

³Cold Spring Harbor Laboratory, Cold Spring Harbor, NY 11724, USA

⁴School of Agriculture, Sun Yat-Sen University, Shenzhen 518107, China

⁵These authors contributed equally to this article.

*Correspondence: Fang Yang (fyang@mail.hzau.edu.cn)

<https://doi.org/10.1016/j.molp.2024.06.007>

ABSTRACT

Maize develops separate ear and tassel inflorescences with initially similar morphology but ultimately different architecture and sexuality. The detailed regulatory mechanisms underlying these changes still remain largely unclear. In this study, through analyzing the time-course meristem transcriptomes and floret single-cell transcriptomes of ear and tassel, we revealed the regulatory dynamics and pathways underlying inflorescence development and sex differentiation. We identified 16 diverse gene clusters with differential spatiotemporal expression patterns and revealed biased regulation of redox, programmed cell death, and hormone signals during meristem differentiation between ear and tassel. Notably, based on their dynamic expression patterns, we revealed the roles of two RNA-binding proteins in regulating inflorescence meristem activity and axillary meristem formation. Moreover, using the transcriptional profiles of 53 910 single cells, we uncovered the cellular heterogeneity between ear and tassel florets. We found that multiple signals associated with either enhanced cell death or reduced growth are responsible for tassel pistil suppression, while part of the gibberellic acid signal may act non-cell-autonomously to regulate ear stamen arrest during sex differentiation. We further showed that the pistil-protection gene *SILKLESS 1 (SK1)* functions antagonistically to the known pistil-suppression genes through regulating common molecular pathways, and constructed a regulatory network for pistil-fate determination. Collectively, our study provides a deep understanding of the regulatory mechanisms underlying inflorescence development and sex differentiation in maize, laying the foundation for identifying new regulators and pathways for maize hybrid breeding and improvement.

Key words: maize, inflorescence, floral organ, sex differentiation, single-cell RNA sequencing, RNA-binding protein

Sun Y., Dong L., Kang L., Zhong W., Jackson D., and Yang F. (2024). Progressive meristem and single-cell transcriptomes reveal the regulatory mechanisms underlying maize inflorescence development and sex differentiation. *Mol. Plant.* **17**, 1019–1037.

INTRODUCTION

Maize develops male and female inflorescences, called tassel and ear, showing great divergence in morphology and sexuality. Interestingly, they have highly similar morphology and differentiation processes at the early stage: apical inflorescence meristem

(IM) differentiates spikelet pair meristem (SPM), which develops two spikelet meristems (SMs), and each SM will continue to

Published by the Molecular Plant Shanghai Editorial Office in association with Cell Press, an imprint of Elsevier Inc., on behalf of CSPB and CEMPS, CAS.

Molecular Plant 17, 1019–1037, July 1 2024 © 2024 The Author. 1019

This is an open access article under the CC BY-NC-ND license (<http://creativecommons.org/licenses/by-nc-nd/4.0/>).

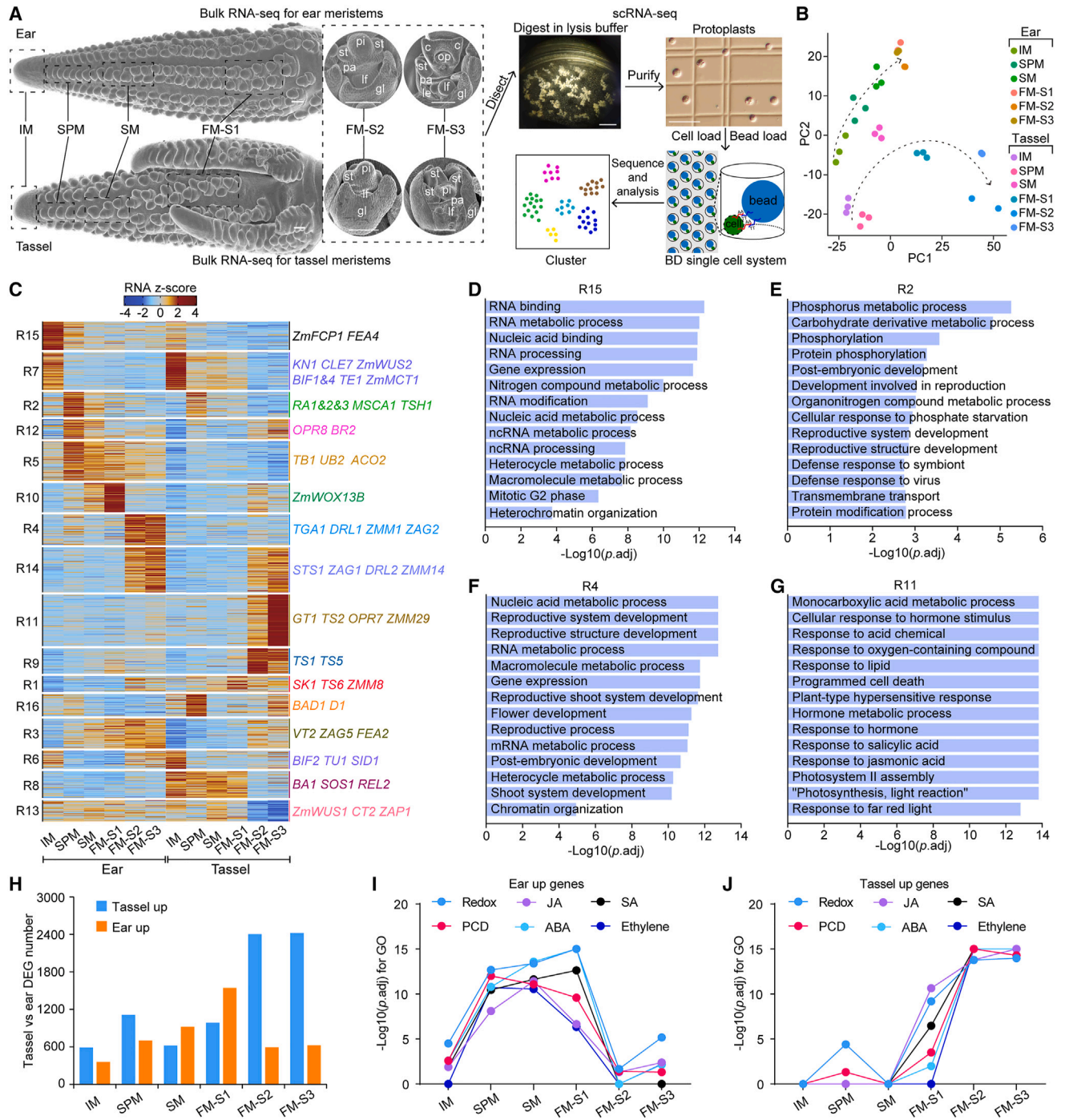


Figure 1. Overview of transcriptomic dynamics during inflorescence meristem differentiation.

(A) Experimental design. The different types of meristems were excised with a razor blade for bulk RNA-seq, and the FM stages S2 (prior to pistil suppression) and S3 (during pistil suppression) were used for protoplast extraction and scRNA sequencing. IM, inflorescence meristem; SPM, spikelet pair meristem; SM, spikelet meristem; FM-S1, floral meristem at stage 1; FM-S2, FM at stage 2; FM-S3, FM at stage 3. pi, pistil; c, carpel; op, ovule primordia; st, stamen; le, lemma; pa, palea; gl, glume; lf, lower floret. Scale bars in SEM images, 150 μm ; scale bars in lysis buffer image = 5 mm and in protoplast image = 50 μm .

(B) Principal component (PC) plot of bulk RNA-seq data shows high concordance between replicates. The directions from IM to FM-S3 are indicated by a virtual arc with an arrow.

(C) Heatmap of differentially expressed genes (DEGs) sorted by *k*-means clustering across the different meristems. The representative genes are shown on the right.

(legend continued on next page)

develop upper and lower floral meristems (FMs) (Chen and Gallavotti, 2021). During floret development, both upper and lower florets develop normally in the tassel, whereas only the upper floret continues to grow and produce kernels in the ear. The tassel primordium also produces branch meristem (BM) at the early stage, leading to a morphology totally different from that of ear. The differentiated axillary meristems undergo further indeterminate (SPM, SM, and BM) or determinate (FM) growth, under elaborate controls, to shape the inflorescence architecture. The *KNOTTED1* (*KN1*) and classic *CLAVATA* (*CLV*)–*WUSCHEL* (*WUS*) negative feedback loop are critical for meristem maintenance (Jackson et al., 1994; Fletcher, 2018). Auxin signaling genes *SPARSE INFLORESCENCE1* (*SPI1*), *VANISHING TASSEL2* (*VT2*), *BARREN INFLORESCENCE 1* (*BIF1*), *BIF2*, *BIF4*, and *BARREN STALK 1* (*BA1*) are expressed in IM periphery and/or axillary meristem and are required for axillary meristem initiation (Gallavotti et al., 2004, 2008; McSteen et al., 2007; Phillips et al., 2011; Galli et al., 2015). The axillary meristem determinacy is controlled by classic *BRANCHED SILKLESS 1* (*BD1*) and *RAMOSA* (*RA1*, *RA2*, and *RA3*) genes (Chuck et al., 2002; Vollbrecht et al., 2005; Bortiri et al., 2006; Satoh-Nagasawa et al., 2006). Further floral organ formation and development are determined by *MADS-box* and *YABBY* genes (Ambrose et al., 2000; Thompson et al., 2009; Bartlett et al., 2015; Strable and Vollbrecht, 2019). However, the molecular profiles responsible for the divergent morphologies between ear and tassel are largely unknown.

In nature, maize represents a unique monoecious species bearing separate male and female flowers. Both tassel and ear florets initiate a full set of floral organs, but the pistils of tassel florets and the stamens of ear florets degenerate, leading to unisexual flowers. The typical tassel-seeded mutants (*TS1*–*6*) produce kernels in the tassel due to a failure of pistil degeneration (Li and Liu, 2017). *TS1* and *TS2* encoding lipoxygenase and short-chain alcohol dehydrogenase, respectively, are involved in jasmonic acid (JA) biosynthesis, suggesting that JA is important in maintaining tassel masculinization (DeLong et al., 1993; Acosta et al., 2009). A recent study found that expression of the classical maize tillering gene, *GRASSY TILLERS 1* (*GT1*), and an ear branching suppressor, *RA3*, in pistil primordia of tassel florets suppresses their growth (Klein et al., 2022). In contrast, *SILKLESS 1* (*SK1*), encoding a uridine diphosphate (UDP)-glycosyltransferase, functions to protect pistil growth in ear (Hayward et al., 2016). On the other hand, for the stamen arrest in ear florets, gibberellic acid (GA) is known to have roles, based on the fact that *dwarf1* (*D1*), *D3*, *D8*, *D9*, and *anther ear 1* (*an1*) mutants with defective GA signaling have stamens in ear florets (Bensen et al., 1995; Winkler and Helentjaris, 1995; Kim et al., 2007; Lawit et al., 2010; Chen et al., 2014). Besides, GA can promote the growth of tassel pistil based on the GA treatment experiments (Nickerson, 1959; Best et al., 2016). In contrast to GA, brassinosteroid (BR) is a hormone that positively regulates stamen maturation and pistil arrest in tassel, and the reported genes include *NANA PLANT 1* (*NA1*), *NA2*, and *BRD1* (Hartwig et al., 2011; Makarevitch et al., 2012; Best et al., 2016). The sex

differentiation of maize is under fine and complex control; however, the processes driving cell-fate change and its molecular mechanism are largely unknown.

Organogenesis and cell-fate determinacy occur in cell types present only in specific sites or at specific stages. The single-cell omics with the ability to differentiate cell heterogeneity provides perfect tools to investigate cell-fate determinacy at the single-cell level. Currently, single-cell RNA sequencing (scRNA-seq) has been successfully applied to map meristem structure and trajectory in different species and tissues including the shoot apical meristem, root tip, inflorescence, and flowers (Zhang et al., 2019, 2021; Satterlee et al., 2020; Xu et al., 2021; Zong et al., 2022; Li et al., 2023) and deepens our understanding of cell-fate determination. In this study, we unravel transcriptomic dynamics during inflorescence axillary meristem differentiation, with a focus on the later floret sex differentiation stage at the single-cell level. Our findings provide a comprehensive view about molecular basis of inflorescence development and sex differentiation in maize.

RESULTS

Transcriptomic dynamics during ear and tassel inflorescence development

The development of maize ear and tassel inflorescences starts with similar morphology and program but later diverge greatly and determines the grain number and pollen quantity, respectively. To explore the regulatory mechanisms responsible for this divergence, we first generated spatiotemporal transcriptome data by finely dissecting different inflorescence meristems, including IM, SPM, SM, FM stage 1 (FM-S1) with flower meristem, FM-S2 with visible floral organs, and FM-S3 with sexual organs being suppressed, of both ear and tassel (Figure 1A and Supplemental Table 1). Principal component analysis (PCA) of these 12 samples showed high concordance between replicates and differences between tissues (Figure 1B). The known genes, such as *FCP1*, *CLE7*, *RAMOSAs*, *BD1*, and some *MADS-box* genes, showed expected expression patterns (Supplemental Figure 1A) (Ambrose et al., 2000; Chuck et al., 2002; Vollbrecht et al., 2005; Bortiri et al., 2006; Satoh-Nagasawa et al., 2006; Thompson et al., 2009; Bartlett et al., 2015; Je et al., 2016; Strable and Vollbrecht, 2019; Liu et al., 2021). These results demonstrate that our fine dissection could separate these 12 types of inflorescence meristems present in ear and tassel along the developmental progress.

To investigate spatiotemporal transcription dynamics, we used *k*-means clustering to sort all differentially expressed genes (DEGs) obtained by comparing any two of the 12 tissues from ear and tassel. This resulted in 16 clusters, which we named R1 to R16, respectively (Figure 1C and Supplemental Table 1). These clusters exposed diverse expression patterns along the developmental stages in and also between ear and tassel (Figure 1C), and genes in different clusters were involved in different pathways based on gene ontology (GO) analysis (Figure 1D–1G and Supplemental Figure 1B). For example,

(D–G) GO analyses of four RNA-seq clusters (R15, R2, R4, and R11). The top 14 representative GO terms are shown.

(H) The DEG numbers of parallel meristem comparisons between ear and tassel. The DEGs were defined by $p_{\text{adj}} < 0.01$ and $|\text{fold change}| > 2$.

(I and J) The significance of correlated GO terms for redox, programmed cell death (PCD), and four hormone signals are higher in early-stage ear meristems (IM, SPM, and SM) **(I)** and in later-stage tassel meristems (FM-S2 and FM-S3) **(J)**.

Molecular Plant

clusters R15 and R7 were IM-enriched and mainly involved in RNA binding and modification and cell-cycle processes (Figure 1D and Supplemental Figure 1B). Clusters R2 and R12 were SPM-enriched and involved in protein kinase activity and phosphorylation (Figure 1E and Supplemental Figure 1B). Notably, some meristem clusters were present specifically in ear or tassel; for example, clusters R4, R5, and R10 were specific in ear, whereas clusters R8, R9, R11, and R16 were specific in tassel (Figure 1C). This result supports the idea that ear and tassel inflorescences undergo different differentiation programs responsible for the divergent architectures. Meanwhile, ear and tassel also shared some common clusters, such as clusters R2, R7, and R14, indicating that they also share some common differentiation pathways (Figure 1C). Interestingly, the genes in clusters R4, R9, R11, and R14 were rapidly activated at the FM-S2 stage when floral organs formed (Figure 1C). Among these, cluster R4 genes were preferentially expressed in ear florets and were involved in nucleic acid metabolic and floral whorl development processes (Figure 1F and Supplemental Figure 1B). In contrast, clusters R9 and R11 were preferentially expressed in tassel florets and enriched in processes of oxygen-containing compound and hormone responses and programmed cell death (PCD) (Figure 1G and Supplemental Figure 1B). These results imply that tassel florets have unique differentiation characteristics compared with ear florets. Among these genes were ones with important roles in pistil arrest, including *TS1*, *TS2*, *OXO-PHYTODIENOATE REDUCTASE7 (OPR7)*, and *GT1* (Figure 1C) (DeLong et al., 1993; Acosta et al., 2009; Yan et al., 2012; Klein et al., 2022). Our data reveal the dynamic transcriptional controls during the consecutive meristem differentiations in/between ear and tassel.

To further explore the molecular basis for the divergence between ear and tassel, we investigated the DEGs for each type of meristem between ear and tassel, e.g., between ear IM and tassel IM (Supplemental Table 1). We identified 948–1816 DEGs for early-stage meristems (IM, SPM, and SM), demonstrating a considerable molecular difference despite their morphological similarity between ear and tassel (Figure 1H). More genes (2530–3050) were differentially expressed at the later stage when flowering started. GO analysis showed that the genes related to flower development were enriched in ear at FM-S2 and FM-S3 (Supplemental Figure 2). Surprisingly, the genes related to redox, PCD, and hormones including JA, abscisic acid (ABA), salicylic acid (SA), and ethylene were enriched firstly in ear at IM, SPM, and SM, whereas they later became enriched in tassel at FM-S2 and FM-S3 (Figure 1I and 1J). This result suggests that the effects of redox, PCD, and hormone signals on meristem development undergo a shift between ear and tassel when floral organs initiate.

In summary, we profiled the spatiotemporal gene expression dynamics and revealed the molecular pathways related to the differentiation of different axillary meristems, with a particular focus on the divergent differentiation of FM between ear and tassel.

Meristem activity and axillary meristem formation controlled by RNA-binding proteins

Our spatiotemporal transcriptome data showed that the genes in IM-enriched clusters R15 and R7 were strongly enriched in RNA

Maize inflorescence and sex differentiation

binding, processing, and modification-related pathways (Figure 1D and Supplemental Figure 1B), which inspired us to explore the function of RNA-related genes in the development of IM. *TERMINAL EAR 1 (TE1)* encoding an RNA-binding protein is known to regulate leaf initiation, internode elongation, and tassel feminization (Veit et al., 1998; Wang et al., 2022). It belonged to the cluster R7 (Figure 1C) and was highly expressed in IM and SPM (Figure 2A). RNA *in situ* hybridization confirmed this and also detected its transcripts in the cells at the SPM boundary where the bracts originate (Figure 2B). To identify its function in inflorescence development, we obtained a mutant allele with mutator transposon insertion, *te1-mum4*. This mutant exhibited the defects similar to what has been reported, including tassel feminization (Supplemental Figure 3A–3E). Importantly, we found that *te1-mum4* mutant ears had significantly smaller IMs and overgrown bracts (Figure 2C and 2D), demonstrating its previously undescribed roles in IM activity and bract suppression. In addition to *TE1*, we found that its paralog *ZmMCT1*, which is a homolog of *Arabidopsis Mei2 C-terminal RRM only 1 (MCT1)*, was also present in the IM-enriched cluster R7 (Figure 1C) and exhibited a dynamic expression pattern similar to that of *TE1* (Figure 2A). RNA *in situ* hybridization revealed its specific expression in the IM and SPM, resembling that of *TE1*, but not in the cells at the SPM boundary (Figure 2E). We next obtained three mutant alleles of *ZmMCT1* using CRISPR-Cas9-mediated genome editing (Supplemental Figure 3F). Interestingly, the IM of *zmmct1* ear also became smaller compared to wild type (WT) (Figure 2F), similar to the *te1* mutant. Furthermore, *zmmct1* developed barren inflorescence, including missing SPMs and single row of SMs, and, thus, less kernels (Figure 2G), demonstrating the function of *ZmMCT1* in SPM initiation and differentiation. However, unlike *te1*, the bracts of *zmmct1* were normal (Figure 2G), which is in line with the lack of *ZmMCT1* expression in the boundary regions where the bracts originate. In summary, our dynamic spatiotemporal transcriptome analyses led to a discovery of important roles for two RNA-binding proteins, *TE1* and its paralog, in meristem activity and axillary meristem initiation and branching.

scRNA-seq revealed cellular heterogeneity between ear and tassel floral organs

Maize female and male florets are morphologically similar when floral organs form (FM-S2 stage) but undergo selective suppression of stamen or pistil during further development (FM-S3 stage) in ear and tassel, respectively. Our analyses above revealed the molecular features and differences during these processes (Figure 1C and 1H). To accurately explore the underlying mechanisms, we further performed scRNA-seq using ear and tassel florets at FM-S2 and FM-S3 stages (Figure 1A) and obtained 5700–7700 cells for each sample with median unique molecular identity (UMI) counts of 7996–10 825 and median expressed genes of 3707–4853 after quality control (Supplemental Figure 4A–4C and Supplemental Table 2). Two replicates of each sample showed good reproducibility, and the correlations between scRNA-seq and bulk RNA-seq data were high ($0.82 < r < 0.88$) (Supplemental Figure 4D–4F), revealing good quality of our scRNA-seq data. The effects of protoplasting and cell cycle on cell clustering were mitigated using the protoplasting-induced genes generated from in-parallel pool

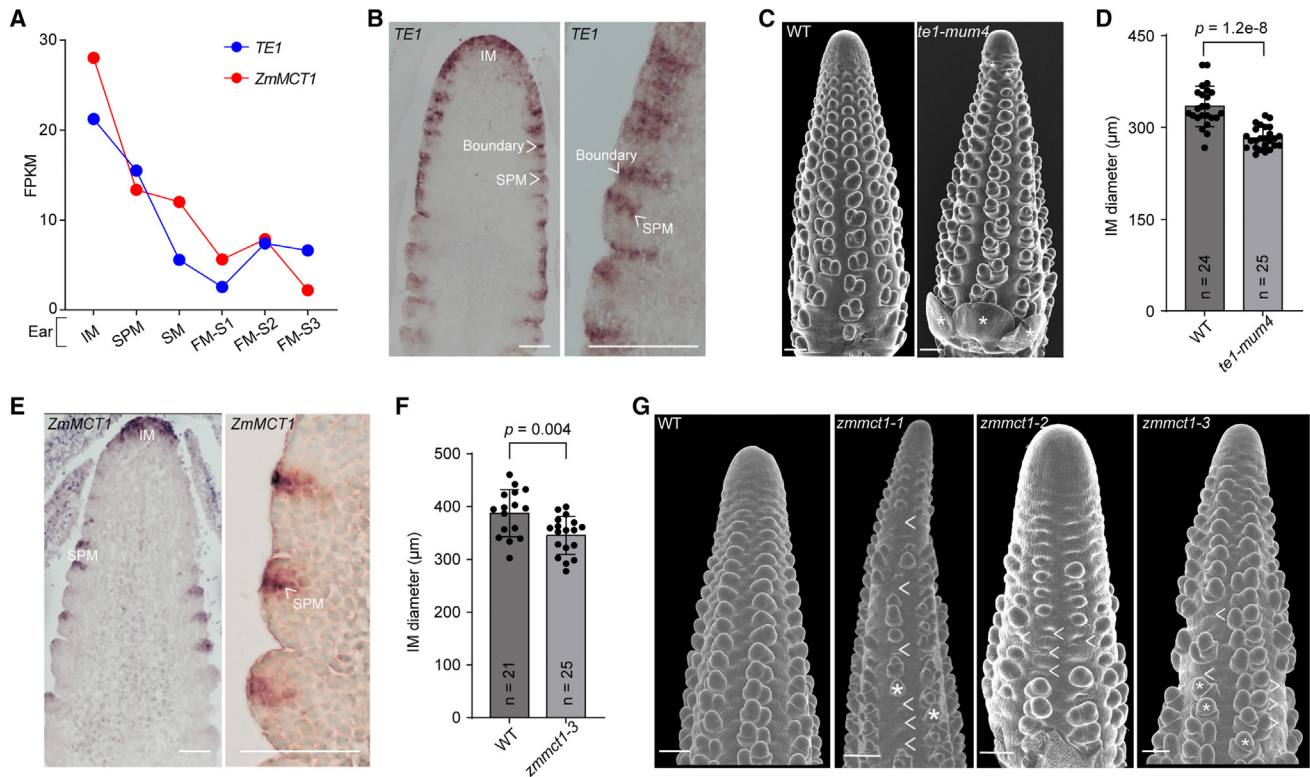


Figure 2. RNA-binding proteins function in meristem activity and axillary meristem formation.

(A) Paralogous RNA-binding proteins *TE1* and *ZmMCT1* are enriched in ear IM and SPM. (B) *TE1* is expressed in IM, SPM, and cells at the SPM boundary. Scale bars, 100 μm . (C) The *te1-mum4* mutant has obvious bract outgrowth (asterisk). Scale bars, 200 μm . (D) *te1-mum4* mutants have smaller IM in comparison to wild type (WT). Data are shown as mean \pm SD; dots show data distribution ($n \geq 20$ biologically independent samples); p value calculated using two-tailed t -test. (E) *ZmMCT1* is expressed in IM and SPM. Scale bars, 100 μm . (F) *zmmct1* mutants have smaller IM in comparison to WT. (G) *zmmct1* mutants have obvious defects in SPM initiation and differentiation. Arrowheads mark defective SPMs, and asterisks mark single SMs. Scale bars, 200 μm .

RNA-seq and cell-cycle genes (Supplemental Table 2) by a standard pipeline provided by Seurat (Stuart et al., 2019). Finally, we merged 53 910 high-quality cells for next cell clustering and annotation.

PCA and unsupervised analyses identified 15 primary clusters that could be classified into six populations using the uniform manifold approximation and projection (UMAP) algorithm (Becht et al., 2019). The populations included vascular cell (VC), epidermal cell (EC), pith/cortex cell (PC), cell-cycle cell (CC), leaf-like cell (LC), and floral organ cell (FC) (Supplemental Figure 5A). The VC population contained cluster 8 and included phloem-specific gene *ALTERED PHLOEM DEVELOPMENT* (*ZmAPL1*), xylem gene *TARGET OF MONOPTEROS5-LIKE 3* (*ZmTMO5-LIKE3*), and confirmed vasculature marker gene *Zm00001d015737* (Supplemental Figure 5B and 5C; Supplemental Table 2) (Xu et al., 2021). The EC population consisted of clusters 4, 5, 7, and 14, in which epidermis-specific genes *LIPID TRANSFER PROTEIN 2* (*LTP2*) and *PROTODERMAL FACTOR 1* (*PDF1*) were highly enriched (Supplemental Figure 5B and 5C) (Xu et al., 2021; Zhang et al., 2021). Pith marker *NAC122* and cortex marker *Zm00001d002347* were detected in the PC population (cluster 6) (Supplemental Figure 5B) (Xu et al., 2021).

This annotation was further confirmed by expression of new marker genes *BENZOAZINONE SYNTHESIS 3* (*BX3*) and *PHOSPHOETHANOLAMINE N-METHYLTRANSFERASE 3* (*PEAMT3*) (Supplemental Figure 5C). The CC population including clusters 9, 11, 12, 13, and 15 were highly enriched for cell-cycle genes, such as *ZmHISTONE2B1* (*ZmHIS2B1*), *ZmHIS2B2*, and *ZmCYCLINB1;2* (*ZmCYCB1;2*) (Supplemental Figure 5B). The glume/lemma/palea genes *ZmYAB8* and *ZmYAB14* were enriched in the LC population (cluster 10) (Supplemental Figure 5B and 5C) (Xu et al., 2021). Lastly, the FC population consisted of clusters 1, 2, and 3, and included meristem, pistil, stamen, and lodicule cells. The meristem gene *KN1* and floral whorl B, C, D, and E class genes, such as *SILKY 1* (*SI1*), *STERILE TASSEL SILKY EAR 1* (*STS1*), *ZAG1*, *ZAG2*, *ZMM27*, and *BEARDED EAR 1* (*BDE1*), were enriched in clusters 2 and 3 (Supplemental Figure 5B and 5C) (Jackson et al., 1994; Theißen et al., 1995; Ambrose et al., 2000; Laudencia-Chingcuanco and Hake, 2002; Thompson et al., 2009; Bartlett et al., 2015; Strable and Vollbrecht, 2019). Cluster 1 was marked by the marker gene *PYRUVATE KINASE 2* (*PYK2*) expression in pistil and stamen of florets (Supplemental Figure 5B and 5C). Taken together, our single-cell annotation could recognize the cells in different domains of floral organs with high heterogeneity.

Sex divergence between ear and tassel happens during development of sex organs. Due to the strong heterogeneity of VCs, ECs, and CCs, our primary clustering failed to distinguish specific floral organs, and information related to sex differentiation was missing. Thus, we further subclustered the cells related to floral organs, glume/lemma/palea, and pith/cortex from primary clusters 1, 2, 3, 6, and 10, and revealed 20 subclusters (Figure 3A). Subcluster 6 was strongly marked by floral whorls B, C, D, and E class genes and shared similar cell percentage between ear and tassel, and thus was labeled as a common floral organ (Figure 3B–3D). Interestingly, some subclusters were specifically enriched in ear or tassel florets, including ear-enriched subclusters 5, 7, 12, 14 and 19, and tassel-enriched subclusters 4, 8, 11, 13, 18, and 20 (Figure 3B and 3C). These subclusters represented the cell heterogeneity between ear and tassel floral organs and might be related to sex differentiation. Subclusters 11 and 12 were named as meristem based on the expression of meristem gene *KN1* (Jackson et al., 1994) and the pistil-protection gene *SK1* (Hayward et al., 2016) in the meristem region detected by *in situ* hybridization (Figure 3D and 3E). *SK1* was also expressed in developing ear pistil and was present in ear subcluster 5, which showed expression of floral whorl genes *STS1*, *BDE1*, *ZMM8*, and *ZMM14* (Figure 3E; Supplemental Figures 6 and 7). Subcluster 5 was ear-enriched, and *SK1* functions to protect pistil growth; thus, subcluster 5 might represent ear pistil cells. Adjacent to subcluster 5, the tassel-enriched subcluster 13 contained the pistil-suppressor genes *TS1*, *TS2*, and *GT1*, and the new marker genes, *NAC2* and *TREHALOSE-6-PHOSPHATE PHOSPHATASE 11* (*TPP11*), were specifically and highly expressed in pistil of tassel (Figure 3D and 3E; Supplemental Figures 6 and 7). Thus, subcluster 13 might represent tassel pistil cells. *TS1* and *TS2* were also expressed in stamen primordia in tassel and marked tassel-enriched subclusters 4, 8, and 18 (Figure 3D and 3E). Moreover, two other marker genes from these clusters, *VIVIPAROUS12* (*VP12*) and *WRKY64*, were experimentally validated to express in stamen primordia of tassel (Figure 3D and 3E). In addition, *VP12* was also expressed in ear stamen at a later stage (Figure 3E) and was enriched in ear-enriched subcluster 14 in separated ear data (Figure 3B; Supplemental Figures 6 and 7), indicating that subcluster 14 might be related to suppressed ear stamen. We thus named subclusters 4, 8, 14, and 18 as stamen cells. In summary, we identified subclusters containing different floral organs and revealed the heterogeneity of meristem, pistil, and stamen cells between ear and tassel.

Enhanced cell death and reduced growth signals are responsible for tassel pistil suppression

To explore the molecular pathways of different pistil fates in ear and tassel, we next analyzed the DEGs for pistil cells (subclusters 5 and 13) from ear and tassel across different stages. We identified 2666, 2726, and 288 DEGs for tassel versus ear at FM-S2, tassel versus ear at FM-S3, and tassel FM-S3 versus tassel FM-S2, respectively (Figure 4A–4C; Supplemental Table 3). GO analysis found that upregulated genes in these three comparisons were involved in pathways of oxidative stress, respiratory burst, reactive oxygen species (ROS) signaling, and glutathione transferase activity (Figure 4D), suggesting a high ROS level in tassel pistil cells, in line with their cell death fate. Correspondingly, the genes that produce superoxide anions

(O_2^-) were upregulated, including *RESPIRATORY BURST OXIDASE HOMOLOG3* (*RBOH3*), *RBOH4*, and *RBOH15*, while the genes that eliminate O_2^- were downregulated, including *SUPEROXIDE DISMUTASE 2* (*SOD2*), *SOD3*, *SOD4*, *SOD9*, and *SOD14* (Figure 4A–4C) (Choudhury et al., 2017). Two polyamine oxidase genes, *PAO1* and *PAO6*, responsible for hydrogen peroxide (H_2O_2) production, were also upregulated (Figure 4A–4C) (Yoda et al., 2006). Besides, the upregulated genes were also enriched in JA, ABA, and SA signaling (Figure 4D), indicating the hormone roles in tassel pistil arrest. This was supported by their functions in cell death regulation (Calderon-Urrea and Dellaporta, 1999; Brodersen et al., 2005; Cui et al., 2013; Bernacki et al., 2021). Notably, the JA biosynthesis and signaling genes showed general upregulation in tassel pistil and other cell types (Figure 4E), which is in line with the role of JA to trigger pistil cell death during floret development of maize tassel (Acosta et al., 2009; Yan et al., 2012). In addition, the significantly enriched alcohol response pathway supported the idea that the alcohol metabolic process is associated with pistil suppression (Figure 4D). For example, the upregulation of *TS2* encoding an alcohol dehydrogenase functions in pistil cell death (Figure 4E) (DeLong et al., 1993; Calderon-Urrea and Dellaporta, 1999). We further observed that two cysteine proteases, *CCP30* and *CCP31*, were upregulated at FM-S2 (Figure 4A). This type of gene is central in regulating cell death during oxidative stress and pathogen attack in plants (Coll et al., 2010, 2014; Wrzaczek et al., 2015; Salvesen et al., 2016). *NAC* transcription factors have also been widely reported to positively regulate cell death in defense and development processes of plants (Valdivia et al., 2013; Lee et al., 2017; Huysmans et al., 2018; Doll et al., 2023). Here, we detected 14 *NAC* genes being upregulated in tassel pistil at FM-S2 or/and FM-S3 (Figure 4F), and confirmed that *NAC29*, *NAC40*, and *NAC126* could induce cell death in *Nicotiana benthamiana* through transient overexpression (Figure 4G). Together, the upregulation of multiple cell death signals is likely responsible for the pistil suppression in the tassel.

In contrast, the downregulated genes in tassel versus ear pistil cells showed distinct signatures and were enriched in pathways of chromatin remodeling, cell division, cell communication, and flower development (Figure 4D). This was in line with the reduced cell proliferation and development of pistil during suppression in the tassel. Meanwhile, the pistil-protection gene *SK1* was downregulated at FM-S3 (Figure 4E). Cell-wall genes were also related to the pistil suppression of tassel (Figure 4D). Support for this came from the downregulation of cellulose synthase genes *CESA1* and *CESA2* and α/β -expansin genes *EXPA4* and *EXPB2*, together with the upregulation of genes for degrading cellulose and pectin (Figure 4A and 4B), which are the main components of cell wall (Keegstra, 2010).

Interestingly, we found that 79% (384/487) of genes upregulated in tassel compared to ear at FM-S3 were already upregulated at FM-S2 (Figure 4H). These included the pistil-suppression genes *TS1* and *TS2* (Figure 4E), suggesting that the molecular differences underlying pistil suppression of tassel are established before the morphological differences between ear and tassel florets are visible. However, 103 genes were upregulated only at the FM-S3 stage in tassel (Figure 4H and Supplemental Table 3), suggesting their potential functions in pistil suppression specifically in later florets, including the

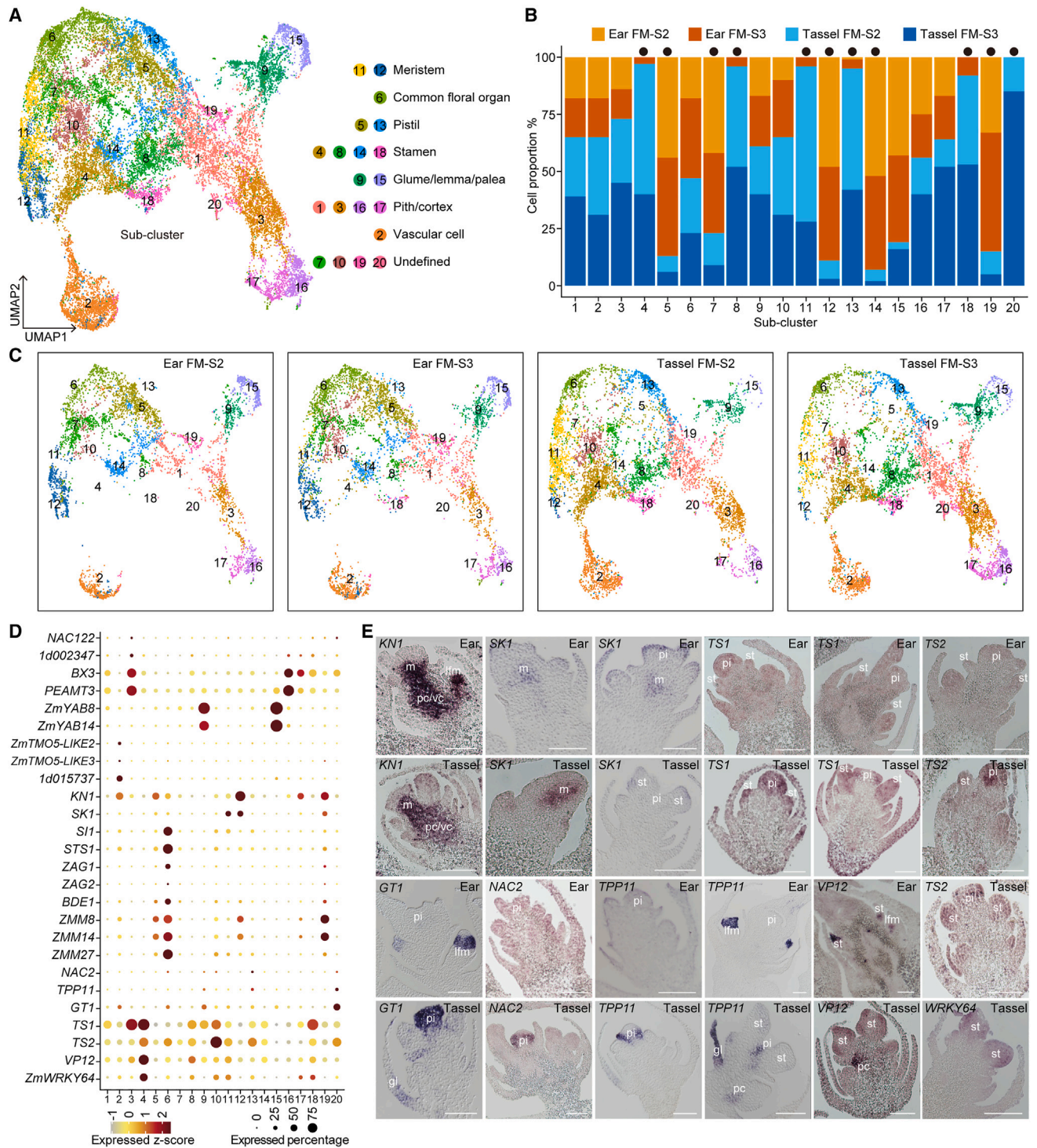


Figure 3. scRNA-seq reveals the cellular heterogeneity between ear and tassel floral organs.

(A) UMAP visualization of 20 subclusters using cells from floral organs, pith/cortex, and palea/lemma/glume. Dots, individual cells; colors, cell sub-clusters.

(B) The proportions of subcluster cells in ear and tassel at FM-S2 and FM-S3 stages show some relatively ear- or tassel-enriched clusters, which are marked by the black dots on top of the bars.

(C) UMAP plots of subclusters for separated four tissues visualize the relatively tissue-specific clusters.

(D) Expression patterns of marker genes used for cell-type annotations in dot plots. Circle size indicates the percentage of cells expressing the marker, and the colors represent Z-score expression value.

(E) Validation of selected marker genes by RNA *in situ* hybridization. m, meristem; lfm, lower floral meristem; pi, pistil; st, stamen; gl, glume; pc, pith/cortex cell; vc, vascular cell. Scale bars, 100 μ m.

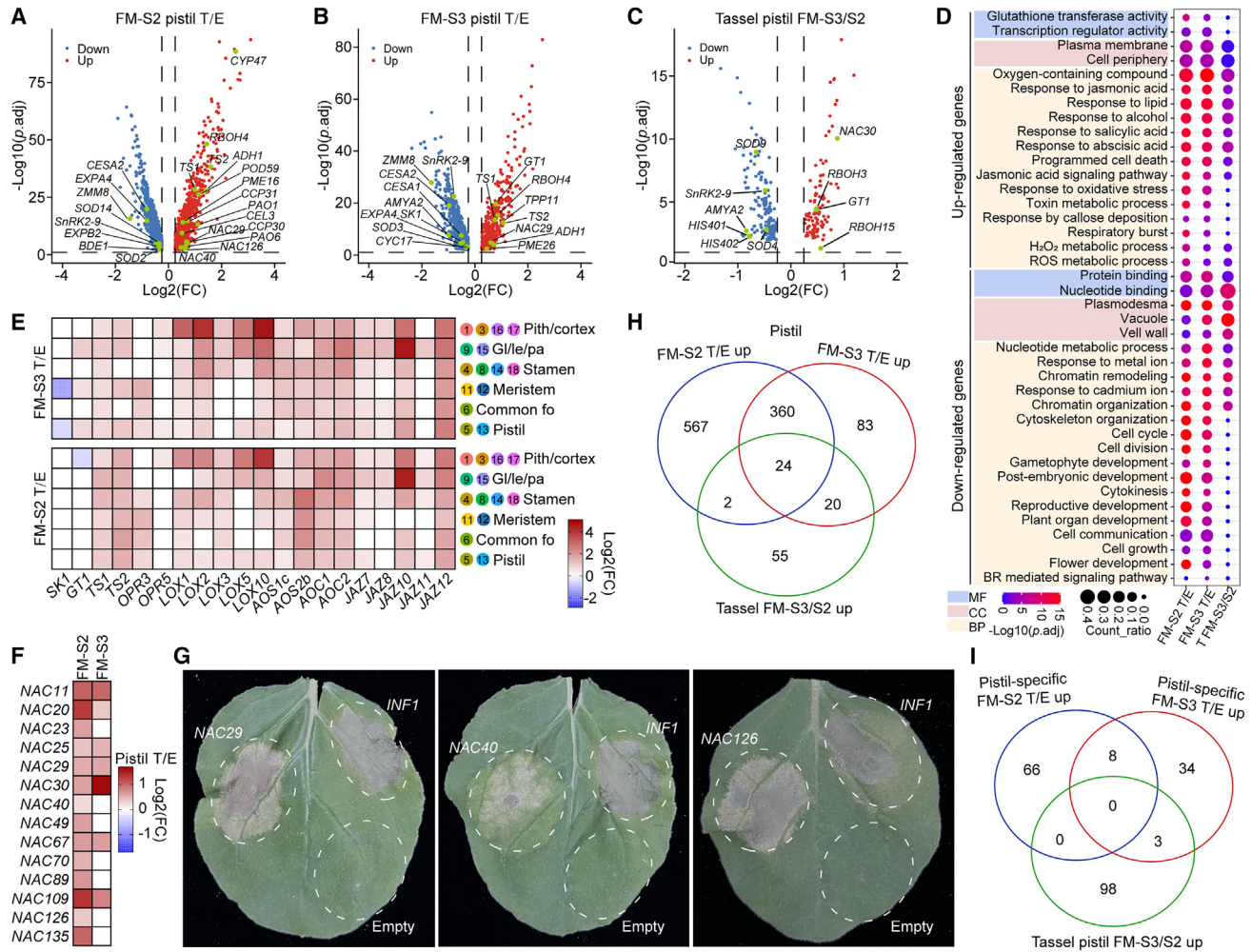


Figure 4. Enhanced cell death and reduced growth signals are likely responsible for tassel pistil suppression.

(A–C) Volcano plots of DEGs for tassel versus ear pistil at the stage of FM-S2 (A), FM-S3 (B), and tassel pistils between FM-S2 and FM-S3 (C). Some representative genes are shown. Dashed lines indicate the thresholds of DEG fold change (FC) and significance. E and T represent ear and tassel, respectively.

(D) The top representative GO terms of up- and downregulated genes for the three comparisons. MF, molecular function; CC, cell component; BP, biological process.

(E) Heatmaps of fold changes for JA signaling genes in different cell types. fo, floral organ; gl, glume; le, lemma; pa, palea.

(F) Heatmap of fold changes for 14 NAC transcription factors that are upregulated in tassel pistils.

(G) Three NAC genes, *NAC29*, *NAC40*, and *NAC126*, can induce cell death in *N. benthamiana* through transient overexpression. This experiment was repeated three times with similar results. As a positive control, *INF1* from the oomycete *Phytophthora infestans*, which is known to induce cell death, was used. The empty vector, without any exogenous gene inserted, was used as the negative control.

(H) Venn plot of tassel pistil upregulated genes at FM-S2 and FM-S3, and FM-S3 tassel pistil upregulated genes relative to FM-S2 tassel pistil.

(I) Venn plot of tassel upregulated pistil-specific DEGs (not differentially expressed in other cell types) at FM-S2 and FM-S3, and FM-S3 tassel pistil upregulated genes relative to FM-S2 tassel pistil.

pistil-suppression gene *GT1* (Figure 4E). To be more specific, we removed the DEGs that were also differentially expressed in other cell types and identified 74 upregulated genes at FM-S2 and 45 at FM-S3 in tassel (Figure 4I; Supplemental Figure 8A and 8B; Supplemental Table 3). These DEGs were pistil specific and may regulate pistil arrest more specifically, including *NAC126*, which was shown to promote cell death in tobacco leaf (Figure 4G).

Taken together, these results reveal the potential molecular pathways for tassel pistil suppression, with the signals associated

with either enhanced cell death or reduced growth playing major roles.

Potential regulators mediate ear stamen arrest

To understand the molecular regulation of stamen arrest in ear, we focused on the stamen cells (subclusters 4, 8, 14, and 18) from ear and tassel florets and identified 4378, 6680, and 406 DEGs for ear versus tassel at FM-S2, ear versus tassel at FM-S3, and ear FM-S3 versus ear FM-S2, respectively (Figure 5A–5C and Supplemental Table 3). The JA signal was again

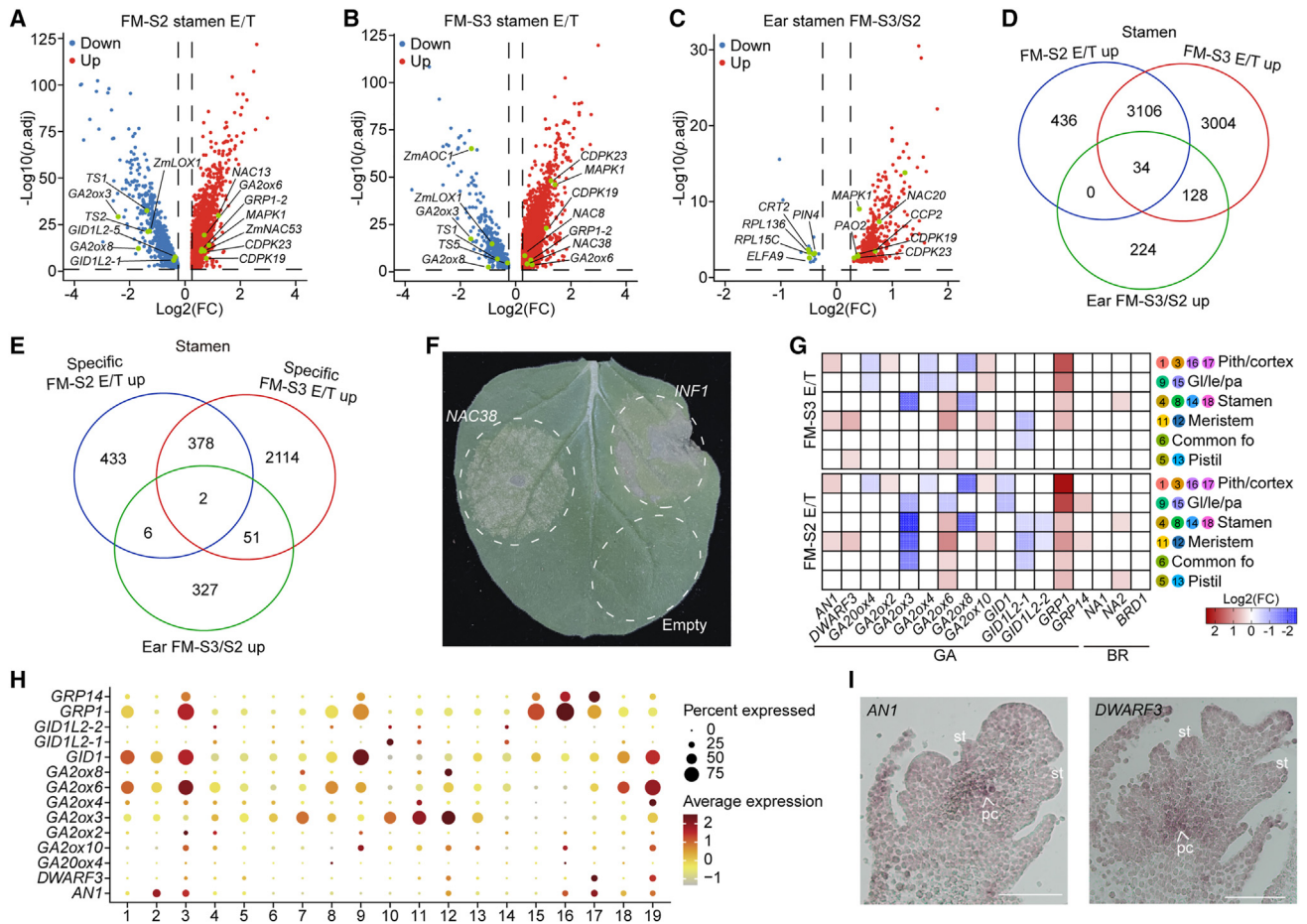


Figure 5. Potential regulators mediate ear stamen arrest.

(A–C) Volcano plots of DEGs for ear versus tassel stamen at the stages of FM-S2 (A), FM-S3 (B), and ear stamen between FM-S2 and FM-S3 (C). Some representative genes are shown. Dashed lines indicate the thresholds of DEG fold change (FC) and significance. E and T represent ear and tassel, respectively.

(D) Venn plot of ear stamen upregulated gene at FM-S2 and FM-S3, and FM-S3 ear stamen upregulated genes relative to FM-S2 ear stamen.

(E) Venn plot of ear upregulated stamen-specific DEGs (not differentially expressed in other cell types) at FM-S2 and FM-S3, and FM-S3 ear stamen upregulated genes relative to FM-S2 ear stamen.

(F) *NAC38* can induce cell death in *N. benthamiana* through transient overexpression. This experiment was repeated three times with similar results.

(G) Heatmaps of fold changes for differentially expressed GA- and BR-related genes in different cell types. fo, floral organ; gl, glume; le, lemma; pa, palea.

(H) Dot plot showing expression patterns of 14 differentially expressed GA-related genes in different cell types. The numbers in x axis representing cell types are listed in Figure 3A.

(I) Expression patterns of sex-regulating genes *AN1* and *DWARF3* in ear florets by RNA *in situ* hybridization. Arrowheads mark the expressed pith/cortex (pc) regions. st, stamen. Scale bars, 100 μ m.

stronger in tassel stamen relative to ear (Figure 4E; Supplemental Figure 9A and 9B), including *TS1* and *TS2* that were confirmed by RNA *in situ* hybridization (Figure 3E). This result suggests that JA signaling could not be responsible for stamen arrest. We then found that the genes encoding protein serine/threonine kinases were over-represented in all three ear upregulated gene sets, including CALCIUM-DEPENDENT PROTEIN KINASE 19 (*CDPK19*), *CDPK23*, and MITOGEN-ACTIVATED PROTEIN KINASE 1 (*MAPK1*) (Figure 5A–5C and Supplemental Figure 9A–9C). *CDPK* and *MAPK* signaling are widely reported to activate PCD in plant immunity (Ren et al., 2002; Kobayashi et al., 2007; Durian et al., 2020), suggesting their potential roles in ear stamen arrest. The upregulated genes from ear stamen FM-S2 to FM-S3 were also enriched in the processes of oxidative stress and ROS response (Supplemental Figure 9C), indicating enhanced

ROS signaling during stamen arrest. Among these genes, 128 were upregulated only at the FM-S3 stage in ear compared to tassel and may have potential functions in stamen arrest at this later stage. These genes included *PAO6*, *HEAT SHOCK PROTEIN 70 (HSP70)*, *MAPK13*, *CDPK32*, and *NAC49* (Figure 5D and Supplemental Table 3). Homologs of these genes were reported to mediate PCD in other contexts (Xanthoudakis and Nicholson, 2000; Ren et al., 2002; Yoda et al., 2006; Kobayashi et al., 2007; Huysmans et al., 2018), indicating their potential roles in stamen arrest. To be more specific, we removed those DEGs that were also differentially expressed in other cell types and identified 819 upregulated stamen-specific DEGs in ears at FM-S2 and 2545 at FM-S3 (Figure 5E; Supplemental Figure 8C and 8D; Supplemental Table 3). These DEGs may specifically regulate stamen arrest, including *NAC38*,

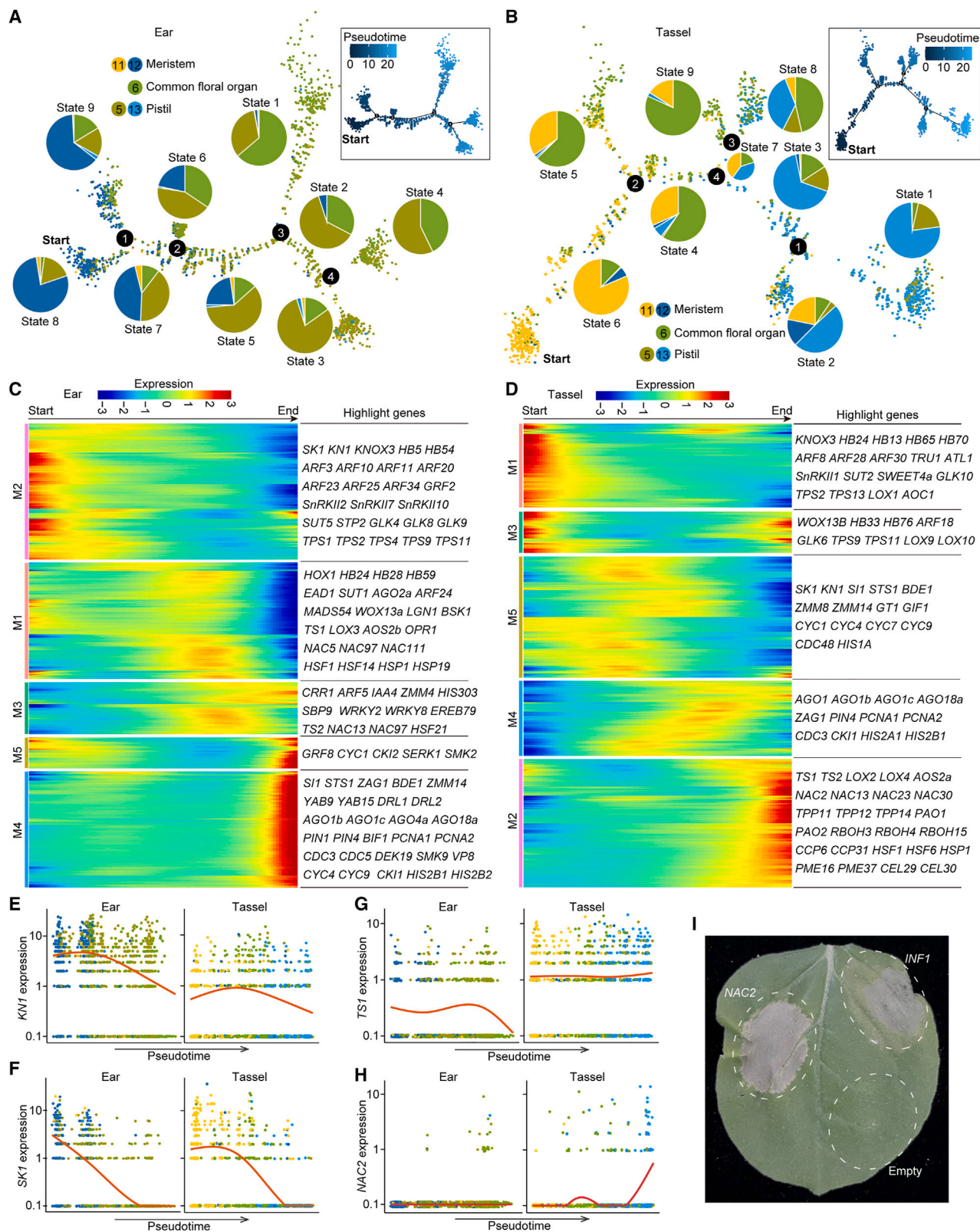


Figure 6. Differentiation trajectories of pistil cells in ear and tassel.

(**A and B**) Differentiation trajectories using pistil-related cells (subclusters 5, 6, 11, 12, and 13) in ear (**A**) and tassel (**B**) show general differentiation from meristem to pistil cells. Colored dots represent cells from different cell clusters. The pie plots show the cell proportions from different cell clusters at each branch state. The pseudotime is shown on the upper right.

(legend continued on next page)

which was confirmed to induce cell death in *N. benthamiana* (Figure 5F). Together, these cell-death-related regulators may mediate ear stamen arrest.

GA signaling plays an important role in ear stamen arrest (Li and Liu, 2017), triggering us to explore the expression dynamics of GA-related genes. We identified six differentially expressed GA-related genes (64 in total) in the stamen and eight genes in other cell types between ear and tassel (Figure 5G). These DEGs had irregular expression dynamics, with seven genes upregulated in the ear and another seven genes upregulated in the tassel (Figure 5G), different from JA-related DEGs which were generally upregulated in all tassel cell types relative to ear (Figure 4E). Surprisingly, these DEGs are not highly expressed in stamen but mainly in pith/cortex and meristem (Figure 5H). For example, *AN1* and *DWARF3*, which are known to suppress ear stamen development, were barely expressed in stamen but rather enriched in the pith/cortex subclusters, which was further confirmed by RNA *in situ* hybridization (Figure 5I). This result suggests that part of the GA signal may act non-cell-autonomously to suppress ear stamen growth.

In contrast to GA, BR was reported to positively regulate stamen maturation and pistil arrest in tassel (Hartwig et al., 2011; Makarevitch et al., 2012; Best et al., 2016), triggering us to look at the BR-related genes. We found that the upregulated genes in tassel stamen or pistil were not enriched in BR-related pathways, but the ear upregulated genes were weakly enriched in BR signaling (Figure 4D; Supplemental Figure 8A and 8B), including the sex-regulating gene *NA2* (Figure 5G) (Best et al., 2016). Other two BR-related genes, *NA1* and *BRD1*, reported to regulate tassel sexuality (Hartwig et al., 2011; Makarevitch et al., 2012), did not show expression differences between ear and tassel (Figure 5G). These results suggest that BR-related genes are not expressed at a higher level in the tassel than in the ear, despite of their regulatory roles in sexuality mainly in the tassel.

Molecular divergence in pistil cell-fate differentiation revealed by differentiation trajectory

To follow the cell-fate transitions during pistil development, we constructed pseudotime trajectories using the pistil-related cells from cell types of meristem (subclusters 11 and 12), common floral organ (subcluster 6), and pistil (subclusters 5 and 13) for ear and tassel, respectively. Both trajectories showed a general differentiation direction from meristem cells to common floral organs and to pistil cells according to the ratios of different cell types in each state (Figure 6A and 6B). The mixed cell types in different states indicated a continuous developmental trajectory during floral organ differentiation. To search for the molecular basis of pistil cell-fate transitions, we further identified the whole-trajectory-dependent and branch-dependent regulators in ear and tassel (Figure 6C and 6D; Supplemental Figure 10A and 10B; Supplemental Table 4). *KN1* and *SK1* were enriched

in the initial pseudotime period, in line with their meristem signatures, but their expression levels were different between ear and tassel (Figure 6E and 6F). Furthermore, the gene modules at the beginning of pseudotime in ear (M2) and tassel (M1 and M3) had 66% different genes (Supplemental Figure 10C). These observations suggest that meristem heterogeneity between ear and tassel was present at the beginning of the cell-fate transition. Next, the middle pseudotime states were classified into two types according to the signatures of branch-dependent regulators in each state. One type was enriched for genes involved in chromatin remodeling, ribosome/RNA biogenesis, and floral whorl development processes, including ear states 2, 6, and 7 and tassel states 3, 5, 8, and 9, while the other was related to oxidoreduction and hormone response, including ear states 1, 5, and 9 and tassel states 4 and 7 (Supplemental Figure 10A and 10B), implying a dual nature of cell differentiation during floral organ development. Finally, major differences between ear and tassel were present at the end of the pseudotime. The ear-enriched genes (M4) showed signatures of cell cycle and were related to reproductive development, including *HIS2B2*, *CYC7/4B*, and some *ARGONAUTE* (*AGO*) and *MADS-box* genes (Figure 6C and Supplemental Figure 11A). In contrast, the tassel-enriched genes (M2) were involved in JA, ABA, SA, and ROS responses and in PCD (Figure 6D and Supplemental Figure 11B), including *TS1* (Figure 6G), which promotes pistil arrest, and *NAC2* (Figure 6H). *NAC2* was activated at the end of tassel pseudotime (Figure 6H) and specifically expressed in the tassel pistil but not in the ear (Figure 3E). We further demonstrated that it can induce cell death in *N. benthamiana* (Figure 3I). Besides, the expression levels of growth-related genes (tassel M4 and M5) were dramatically reduced in tassel when cell differentiation reached the end of the pseudotime (Figure 6D). Together, the cell-differentiation trajectories along pistil development revealed molecular differences that are likely responsible for pistil cell-fate differentiation to continue growth or to be suppressed.

TS1 and *GT1-RA3* module act antagonistically to *SK1* in pistil-fate differentiation through regulating common molecular pathways

To further understand the molecular regulation of pistil-fate determination, we performed a weighted gene co-expression network analysis (WGCNA) to construct regulatory networks of core pistil-suppression genes *TS1*, *TS2*, *GT1*, *RA3*, *OPR7*, and *OPR8*, and the pistil-protection gene *SK1* using all pistil cells (SC5/13) (Supplemental Table 5). The top 400 genes that were positively correlated with the pistil-suppression genes and negatively correlated with *SK1* were used to build the pistil-suppression network (Figure 7A). We found that the genes in this network were enriched in JA/ABA/SA signaling, respiratory burst, and PCD processes (Supplemental Figure 12A), in line with the pistil-suppression function of this network. Notably, *GT1* was linked to *RA3*, *TPP11*, and *NAC25* (Figure 7A). This is supported by previous findings that the pistil outgrowth of *gt1*

(C and D) Expression heatmaps showing five gene modules (M1–M5) of significant DEGs along ear **(C)** and tassel **(D)** pseudotime. Some representative genes in different modules are shown in the table on the right.

(E–H) Scatter plots showing expression dynamics for four representative genes along ear and tassel pseudotime. The colors of the dots correspond to different cell clusters.

(I) *NAC2* can induce cell death in *N. benthamiana* through transient overexpression. This experiment was repeated three times with similar results.

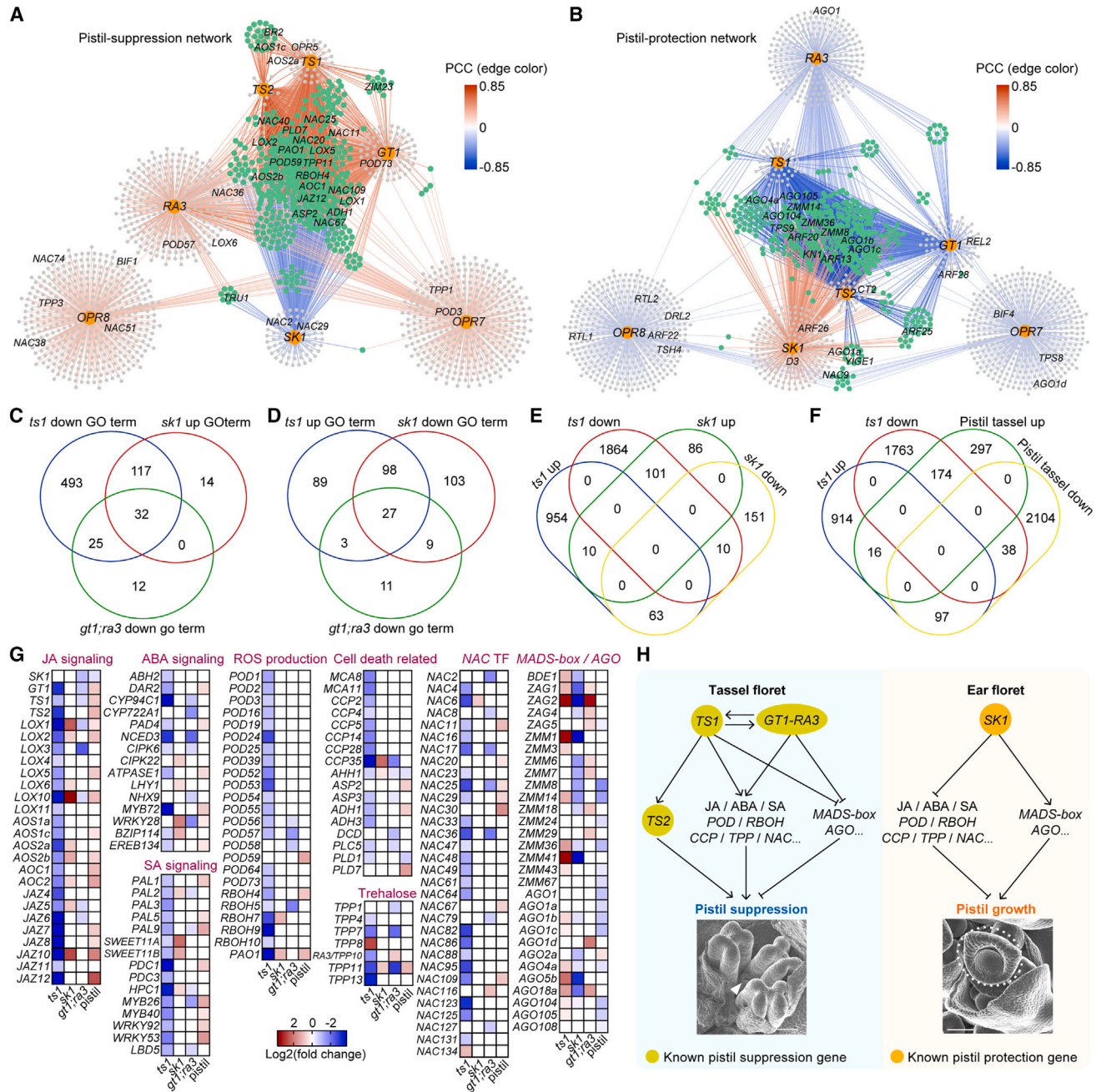


Figure 7. The regulatory network and model for pistil-fate determination.

(A) The pistil-suppression network comprises the top 400 positively co-expressed genes of the pistil-suppression genes *TS1*, *TS2*, *GT1*, *RA3*, *OPR7*, and *OPR8*, and the top 400 negatively co-expressed genes of the pistil-protection gene *SK1*.

(B) The pistil-protection network comprises the top 400 negatively co-expressed genes of *TS1*, *TS2*, *GT1*, *RA3*, *OPR7*, and *OPR8*, and the top 400 positively co-expressed genes of *SK1*. Gray nodes have one edge; green nodes have 2–7 edges; edge color represents Pearson correlation coefficient (PCC).

(C and D) Overlaps of significant GO terms ($p < 0.05$) indicate that *TS1* and *GT1;RA3* act antagonistically to *SK1* through regulating some common molecular pathways.

(E) Overlap of different DEG sets shows that *TS1* and *SK1* tend to antagonistically regulate common gene sets.

(F) Overlap of different DEG sets shows that the upregulated genes in tassel pistil relative to ear pistil tend to be downregulated in *ts1* mutant.

(G) Heatmaps of expression fold changes for eight DEG sets. The JA, ABA, SA, ROS, cell-death-related, and *TPP* and *NAC* genes are generally downregulated in *ts1* and *gt1;ra3* mutants and upregulated in *sk1* mutant and in tassel pistil relative to ear pistil at FM-S3, while *MADS-box* and *AGO* genes exhibit generally opposite dynamics to above genes.

(H) Proposed regulatory models for pistil suppression in tassel florets (left) and pistil growth in ear florets (right). The lines with arrowheads or flat tips correspond to positive or negative regulation, respectively. Triangle and dashed circle in SEM images mark the arrested pistil in tassel floret and the outgrowth pistil in ear floret, respectively. Scale bars, 100 μ m.

mutant tassel was enhanced by *ra3*, while *TPP11* and *NAC25* were downregulated in *gt1;ra3* double mutant (Klein et al., 2022). On the other hand, the top 400 genes that were negatively correlated with the pistil-suppression genes and positively correlated with *SK1* were used to build the pistil-protection network (Figure 7B). Genes in this network were related to cell division and flower development (Supplemental Figure 12B), including many *MADS-box*, *AGO*, and *ARF* genes (Figure 7B), supporting that this network is related to promotion of pistil growth. Interestingly, in both networks, we observed that *TS1*, *TS2*, *GT1*, *RA3*, and *SK1* had many linked genes in common (Figure 7A and 7B; Supplemental Figure 11C and 11D), indicating that they share common pathways during pistil-fate determination.

To further support this hypothesis, we analyzed ethyl methanesulfonate (EMS)-induced *ts1* and *sk1* mutants, which showed derepressed pistil in tassel and eliminated pistil in ear, respectively (Supplemental Figure 13A–13C), consistent with previous reports (Acosta et al., 2009; Hayward et al., 2016). We next performed RNA-seq analysis using the early florets from tassel of *ts1* and ear of *sk1* (Supplemental Figure 13D and 13E). There were 1027 upregulated and 1975 downregulated genes in *ts1* tassel, and 197 upregulated and 224 downregulated genes in *sk1* ear (Supplemental Table 5). The published 319 upregulated and 388 downregulated genes in floret-stage *gt1;ra3* tassel were also applied for subsequent analysis (Klein et al., 2022). GO analysis of the DEGs showed that these genes shared large common downstream pathways. On one side, 91% and 83% of GO terms for *sk1* upregulated and *gt1;ra3* downregulated genes, respectively, overlapped with the GO terms for *ts1* downregulated genes (Figure 7C). These included JA/ABA/SA signaling and PCD genes (Supplemental Figure 13G, 13H, and 13K), similar to the genes enriched in pistil-suppression network and the tassel pistil upregulated genes from the scRNA-seq data (Supplemental Figure 12A and Figure 4D). On the other hand, 53% and 60% of GO terms for *sk1* downregulated and *gt1;ra3* upregulated genes, respectively, overlapped with GO terms for *ts1* upregulated genes (Figure 7D). These include cell differentiation and carpel and flower development genes (Supplemental Figure 13F, 13I, and 13J), similar to the genes enriched in the pistil-protection network and tassel pistil downregulated genes revealed by scRNA-seq (Supplemental Figure 12B and Figure 4D). Further, the *sk1* and tassel pistil upregulated genes shared 51% and 36% with *ts1* downregulated genes, respectively (Figure 7E and 7F). These results suggest that *TS1* and *GT1-RA3* module act antagonistically to *SK1* in pistil-fate determination through regulating some common molecular pathways.

Further analyses led us to find that JA, ABA, SA, ROS, cell-death-related, *TPP*, and *NAC* genes were generally downregulated in *ts1* and *gt1;ra3* mutants, while they were generally upregulated in *sk1* mutants and also in tassel pistil relative to ear pistil from scRNA-seq (Figure 7G). These types of genes were also present in the pistil-suppression network (Figure 7A). We thus propose that these genes represent the positive regulators of pistil suppression. On the other hand, *MADS-box* and *AGO* genes involved in flower development (Ji et al., 2011; Heijmans et al., 2012; Zhao et al., 2023) exhibited dynamics generally opposite to those of the above pistil-suppression genes

(Figure 7G). They were also included in the pistil-protection network (Figure 7B). We thus propose that *MADS-box* and *AGO* genes function positively in pistil growth. In addition, we found that *TS1* can positively regulate *TS2*, *GT1*, and *RA3*, while on the other hand the *GT1-RA3* module can positively regulate *TS1*, suggesting a regulatory module for pistil suppression (Figure 7G). We also found that the JA synthesis and signaling genes, *LOX1/2/6/10*, *AOS2A/2B*, *AOC2*, and *JAZ5/10*, were negatively regulated by pistil-protection gene *SK1* but the JA-synthesis-related genes, *TS1* and *TS2*, which suppress pistil, were not affected (Figure 7G). This suggests that *SK1* could protect pistils by blocking JA signaling, which is independent of *TS1* and *TS2* at transcription level. Together, our analysis reveals a regulatory module to explain how *TS1*, *TS2*, *GT1*, *RA3*, and *SK1* control pistil fate and floral sexuality of maize through dependent or independent interaction (Figure 7H).

DISCUSSION

Grass inflorescences undergo conserved differentiation processes to produce different types of axillary and floral meristems to guarantee efficient reproduction and grain numbers (Du et al., 2022). Maize has two types of inflorescences, male and female, with similar initial morphology but high divergence in architecture and sexuality, which is determined by the sequential axillary meristem differentiation processes. Exploring the underlying molecular mechanisms is not only an important biological question but also provides a valuable basis for ear traits optimization and high yield. However, the high-resolution dynamic transcriptional regulation underlying the different fate transitions is poorly understood.

A recent study presented a single-cell transcriptome atlas of the developing ear inflorescence with focus on identification of cell-type markers and candidate functional studies (Xu et al., 2021). In our study, we focused on the sequential differentiation of axillary meristems (IM, SPM, SM, FM-S1, FM-S2, and FM-S3) to explore the molecular signatures and basis for the divergence of ear and tassel. First, 16 meristem-specific modules involving 22 605 DEGs show highly dynamic expression profiles (Figure 1C), revealing that meristem differentiation is under precise and dynamic control. The meristem-specific modules help reveal potential candidates responsible for meristem differentiation. As a support, we discovered roles for RNA-binding genes, *TE1* and its paralog *ZmMCT1*, enriched in the IM-specific module, in controlling IM activity and axillary meristem formation (Figure 2). *TE1* regulates leaf initiation, internode elongation, and tassel feminization (Veit et al., 1998; Wang et al., 2022), and our discovery of a role in the IM adds to the knowledge of this gene function. Furthermore, we also identified that some ear- and tassel-specific modules appeared at a later floret stage, covering ovule genes *ZMM1* and *ZAG2* in ear and pistil-suppression genes *TS1*, *TS2*, and *GT1* in tassel (Figure 1C) (DeLong et al., 1993; Theißen et al., 1995; Laudencia-Chingcuanco and Hake, 2002; Acosta et al., 2009; Klein et al., 2022). These gene modules are likely to be related to floret morphological differences and sex differentiation. In addition, the early-stage meristems (IM, SPM, and SM) between ear and tassel have similar morphology, but our results showed a considerable molecular difference, which provides information for studying their differential regulation

mechanisms. Interestingly, we found that redox, PCD, and hormone signal regulations on meristem differentiation undergo a shift between ear and tassel when floral organs initiate (Figure 1I and 1J), suggesting that these pathways may play different roles in early-stage ear meristem development and later tassel floret sexuality. Thus, our fine spatiotemporal transcriptomes provide valuable information for understanding the axillary meristem differentiation and the molecular differences underlying the divergence between tassel and ear.

Maize tassel and ear florets are initially bisexual and later undergo divergent sex differentiation through pistil or stamen suppression. Among the few characterized pistil- and stamen-suppression genes, most encode enzymes involved in JA or GA synthesis and metabolism, respectively (DeLong et al., 1993; Bensen et al., 1995; Chuck et al., 2007; Acosta et al., 2009; Yan et al., 2012; Chen et al., 2014; Lunde et al., 2019; Klein et al., 2022). The control of maize sexuality is elaborate, and the molecular regulation mechanisms are largely unknown. scRNA-seq supplies a good opportunity to understand the fate determination of specific cell types. Currently, scRNA-seq in plants is largely focused on annotation of cell types and identification of marker genes (Zhang et al., 2019, 2021, 2023; Satterlee et al., 2020; Xu et al., 2021; Otero et al., 2022; Zong et al., 2022; Li et al., 2023; Liu et al., 2023; Zhu et al., 2023). In this study, we applied scRNA-seq to expose the molecular features for the unique cell fates of maize sexual organs. We found that some subclusters including meristem, pistil, and stamen cells are relatively ear- or tassel-specific (Figure 3B), suggesting an obvious heterogeneity between ear and tassel sexual organs. Our analysis of pistil- and stamen-related cells reveals potential regulators and pathways for sex differentiation. Enhanced cell death (e.g., ROS, PCD, and hormones) and reduced cell growth signals (e.g., cell division and flower development) appear to be mainly responsible for pistil suppression in tassel, and these signals were largely established before the morphological differences between ear and tassel appear. These results were supported by the analysis of developmental trajectories of pistil cells, co-expression, and mutant transcriptomes. In particular, our tobacco experiments suggest that some *NAC* transcription factors may promote pistil arrest through direct cell death induction. In addition, we found that protein serine/threonine protein kinases may be responsible for ear stamen arrest, based on their expression and reported functions in activating PCD (Ren et al., 2002; Kobayashi et al., 2007; Durian et al., 2020). GA is the only known signal to promote ear stamen arrest currently (Li and Liu, 2017), although the mechanisms are still not clear. By deeply investigating the transcriptional features of specific cell types, we found that *AN1* and *D3*, which suppress the stamen of ear, are barely expressed in the stamen of ear but mainly expressed in the pith/cortex (Figure 5G–5I). This phenomenon suggests that part of the GA signal may act non-cell-autonomously to regulate ear stamen arrest. Previous studies also found that GA treatments on the maize growing point could induce pistil growth in tassel (Nickerson, 1959; Best et al., 2016), indicating the positive role of GA on pistil growth. In our data, *D3* and *GRP1* were upregulated in pistil of ear relative to tassel, suggesting their potential function in the growth of ear pistils (Figure 5G).

The JA signal including classical *TS1* and *TS2* genes is the key factor for pistil fate in maize (Li and Liu, 2017). Our analyses

also revealed that most JA-related genes were highly enriched in tassel pistil relative to ear pistil (Figure 4E). However, how JA controls pistil fate is not well understood. By combining our scRNA-seq data and mutant transcriptomes, we proposed a regulatory model composed of genes in JA, cell death, and growth signals for pistil-fate determination (Figure 7H). In tassel floret, *TS1* could promote many other JA-related genes, including *TS2*, to produce a high JA level in tassel pistil for its suppression. Meanwhile, JA likely also regulates trehalose pathway to promote tassel pistil suppression, supported by reduced expression of some *TPP* genes in *ts1* mutant (Figure 7G). Mutation in one of these *TPP* genes, *RA3*, leads to the outgrowth of tassel pistil (Klein et al., 2022). Interestingly, three *TPP* genes are positively regulated by *GT1*/*RA3*, which in turn are positively regulated by *TS1*. Together, these results suggest that JA, trehalose, and the classic vegetative branching gene *GT1* form a module with positive regulation relationship to promote tassel pistil suppression. Except for JA, other hormones, ABA and SA, might also have roles in pistil-fate determination. ABA- and SA-related genes are enriched in tassel pistil and positively regulated by *TS1* (Figure 7G). It has been reported that ABA and SA signaling regulates cell death in stresses (Brodersen et al., 2005; Cui et al., 2013; Bernacki et al., 2021), and our data expose their potential roles in regulating pistil arrest.

In ear floret, *SK1* encoding UDP-glycosyltransferase is the only reported gene for protecting pistils from JA-mediated cell death (Calderon-Urrea and Dellaporta, 1999). We found that many JA synthesis and signaling genes are negatively regulated by *SK1* (Figure 7G), supporting that *SK1* could suppress JA's effect on ear floret to protect ear pistils. However, the expression of JA-synthesis-related genes, *TS1* and *TS2*, are not affected by *sk1* mutation, suggesting that *SK1* blocks of *TS1*- and *TS2*-induced cell death does not happen at the transcription level (Calderon-Urrea and Dellaporta, 1999). In addition, our data also suggest that *SK1* could suppress the abundance of cell-death-related genes, such as ABA/SA/ROS-related genes, *TPP*, *NAC*, and *CCP* (Brodersen et al., 2005; Cui et al., 2013; Choudhury et al., 2017; Huysmans et al., 2018; Van Opdenbosch and Lamkanfi, 2019; Bernacki et al., 2021; Klein et al., 2022). On the other hand, *SK1* could promote flower-development-related genes, such as *MADS-box* and *AGO* genes (Ji et al., 2011; Heijmans et al., 2012). Taken together, our study deepens the knowledge of how JA signaling interacts with the *SK1* protection program to control pistil fate and further determine the sexuality of maize.

In summary, we generated comprehensive spatiotemporal transcriptome maps during maize inflorescence development and a single-cell-resolution transcriptome map of maize florets undergoing sex differentiation. These maps provide information to understand the fate transition of IMs and sex differentiation between ear and tassel and help to identify new regulators and networks that would be beneficial for grain-yield improvement.

METHODS

Plant materials and growth conditions

Young ear and tassel were harvested from maize inbred line B73 grown in the field, and different meristems—IM, SPM, SM, FM-S1, FM-S2, and FM-S3—on ear and tassel were excised with a razor blade for bulk RNA-seq.

This method excluded a large amount of inflorescence axis. Meanwhile, the FM-S2 prior to pistil suppression and FM-S3 during pistil suppression were used for protoplast extraction and scRNA-seq. Part of the purified protoplasts of ear and tassel FM-S3 were retained for bulk RNA-seq and subsequent identification of protoplasting-induced genes. The material stages are as follows: IM, SPM, SM, and FM-S1 from 4–6 mm ear and tassel; FM-S2 from 9–11 mm ear and 8–10 mm tassel; FM-S3 from 16–18 mm ear and 14–16 mm tassel. The bulk RNA-seq data for ear IM, SPM, and SM and tassel IM, SPM, SM, and FM-S1 have three biological replicates, while other bulk RNA-seq and all scRNA-seq data have two replicates. *ts1* and *sk1* mutant seeds with B73 background were obtained from the Maize EMS-induced Mutant Database (Lu et al., 2018). *te1-mum4* seeds with B73/W22 background were from the ChinaMu database (Liang et al., 2019). *ts1*, *sk1* and *te1-mum4* mutants were backcrossed into B73 to clean up the background. The self-cross separated seeds were grown in the field for phenotyping and RNA-seq. A region of the tassels containing only florets for *ts1* and a region of the ears containing only florets for *sk1* were collected for RNA-seq using three or two replicates, respectively. CRISPR-Cas9 technology was used to knock out *ZmMCT1*. Two sgRNAs in exons 1 and 3 (the sequences referred to in Supplemental Figure 3E) were designed based on the B73 reference genome by the CRISPR-P 2.0 web tool (Liu et al., 2017). The sgRNA array cloned into a pGW-Cas9 vector (Char et al., 2017) was delivered into maize C01 inbred by *Agrobacterium* infection. Three alleles were identified by Sanger sequencing and backcrossed with original C01 to clean up the background and obtain cas9-free edited plants. The phenotypes were investigated using self-crossed progenies in T3 or T4 generations. The genotyping information for all mutants is listed in Supplemental Table 6.

Bulk RNA-seq library preparation

The different meristems, retained protoplasts, and mutant samples were flash-frozen with liquid nitrogen immediately after collection. Total RNA of these samples was extracted using Direct-zol RNA Miniprep (Zymo Research), and libraries were constructed using NEBNext Ultra Directional RNA Library Prep Kit or MGIEasy RNA Library Prep Kit according to the manufacturer's instructions.

scRNA-seq library preparation

Protoplasts were prepared as previously described (Satterlee et al., 2020). For each replicate, the freshly dissected FM-S2 or FM-S3 tissues from 15–20 ears or tassels were digested in protoplast lysis buffer for 2 h at room temperature in the dark with gentle shaking. The mixture was then filtered twice through a 30- μ m cell strainer (Sysmex, 04-Q042–2316), and the protoplasts were collected by horizontal centrifugation at 300 g for 3 min at room temperature. The supernatant was gently removed without disturbing the protoplast pellet. Next, the pellet was resuspended and washed two times using protoplast washing buffer (lysis buffer without enzyme) by the same centrifugation condition as before. After washing, the pellet was resuspended into 600 μ l of washing buffer and filtered through a 30- μ m cell strainer to remove adherent multicellular mass. Part of the filtrate was stained with fluorescein diacetate (Sigma, F7378) to check concentration and viability of protoplasts with a hemocytometer under GFP and light microscope, and 20 000 good-quality protoplasts with viability \geq 75% were immediately loaded into the BD Rhapsody single-cell system (BD Life Sciences) to construct an scRNA-seq library according to the instructions. The scRNA-seq libraries were subjected to paired-end sequencing (2 \times 150 bp) using Illumina NovaSeq 6000.

RNA *in situ* hybridization

The early- and floret-stage ears and tassels from the inbred line B73 were used for RNA *in situ* hybridization as described previously (Jackson et al., 1994). To prepare probes for *WOXs*, *ZmMCT1*, and scRNA-seq marker genes, we added T7 promoter sequences CAT TAA TAC GAC TCA CTA TAG GG into reverse primers used to amplify gene-specific PCR products from cDNA templates. Primer sequences for all genes are listed in Supplemental Table 6. Digoxigenin-labeled antisense probes were then

transcribed using an *in vitro* transcription kit (Roche) according to the manufacturer's instructions. The hybridized signals were imaged with a Nikon ECLIPSE DIC microscope.

Transient expression assay in *N. benthamiana*

To determine the function of identified candidates in single-cell analysis, their coding sequences were cloned to obtain constructs driven by the CaMV 35S promoter and terminated by the OCS terminus. The constructs were transformed into the *Agrobacterium* strain GV3101, and the positive clones were inoculated into LB medium at 28°C with shaking. After incubation, the agrobacteria were collected and resuspended using infiltration buffer (10 mM 2-(*N*-morpholino)ethanesulfonic acid, 10 mM MgCl₂, and 0.2 mM acetosyringone). The suspensions were adjusted to OD₆₀₀ of 1 and injected into *N. benthamiana* leaves. The cell death phenotype was observed 3–4 days after injection. As a positive control, *INF1* from the oomycete *Phytophthora infestans*, which is known to induce cell death (Kamoun et al., 1998), was used. The empty vector, without any exogenous gene inserted, was used as the negative control.

Imaging

For scanning electron microscopy (SEM) imaging, the freshly dissected tissues were mounted on stubs with silver conductive paint and then imaged on a JEOL JSM-6390/LV scanning electron microscope. For *sk1* mutant phenotype, the mutant and WT ears at ~4.5 cm in length were harvested to investigate the floret phenotypes, and images were taken using a Nikon SMZ25 stereo microscope. The measurements of IM diameter for *ts1* mutant and WT ears also used a Nikon SMZ25 stereo microscope. The plant images of *te1* mutant and WT were taken using a Nikon D7100 camera. All the mutant and WT phenotypes were investigated in segregating populations.

Bulk RNA-seq analysis

The quality of raw sequencing data was controlled using Trimmomatic (v.0.33) with parameters "LEADING:20 TRAILING:20 SLIDINGWINDOW:4:15 MINLEN:20" (Bolger et al., 2014). The clean data were mapped to the B73 AGPv4 reference genome using HISAT2 with default parameters (Kim et al., 2019). SAMtools (v.1.9) (Li et al., 2009) was then used to obtain uniquely mapped reads with the parameter "rmdup and mapq >10." We used featureCounts (v.1.6.3) (Liao et al., 2014) to measure the abundance of RNA with the parameter "-p." Spatiotemporal cluster analysis was run using the LRT function in DESeq2 (v.1.26) (Love et al., 2014) and sorted by *k*-means method. DEGs between parallel meristems were defined by $p_{\text{adj}} < 0.01$ and [fold change] > 2. The PCA plot was generated by the "PlotPCA function" in DESeq2. GO analysis was performed using TBtools (v.1.120) (Chen et al., 2020). All genome browsers were plotted using pyGenomeTracks (v.3.6) (Ramírez et al., 2018).

scRNA-seq analysis, quality control, and clustering

The UMI-based clean data were mapped to the maize genome utilizing STAR mapping with customized parameters (Dobin et al., 2013) to obtain the UMI counts of each sample. All scRNA-seq preprocessing was performed with Seurat (v.4.3.0) software (Hao et al., 2021). For each sample, we computed metrics of each cell, including the number of unique genes detected (nFeature_RNA), the total molecules detected (nCount_RNA), and the percentage of reads mapping to the mitochondria and chloroplast genome (percent.mt; percent.pt). We then carried out quality control using the following criteria: (1) cells with the number of expressed genes between 1800 and 10 000; (2) cells with UMI count between 2800 and 50 000; (3) genes that were expressed in more than three cells; (4) cells with percent.mt and percent.pt less than 10%; and (5) removing doublets by DoubletFinder (v.2.0.3) (McGinnis et al., 2019). Next, eight high-quality datasets were integrated using the "FindIntegrationAnchors" and "IntegrateData" functions in Seurat, after which the effects of protoplasting and cell cycle were regressed by the "ScaleData" function with parameter "vars.to.regress" using protoplasting-induced and cell-cycle genes (Supplemental Table 2).

Protoplasting-induced genes were obtained by a DEG analysis between protoplasts and tissues before protoplasting with screening criteria $p_{\text{adj}} < 0.05$ and $|\log_2\text{fold change}| > 2$. The marker genes with $p_{\text{adj}} = 0$ and $\text{avg}_{\log_2\text{fold change}} > 0.5$ in pre-cluster of cell cycle were defined as cell-cycle genes in florets. For clustering, the dimensions of the expression matrix were reduced by the “RunPCA” function, and the top 15 dimensions were used for “FindNeighbors” and UMAP analysis (Becht et al., 2019). The primary cell clusters were identified by the FindClusters function with a resolution of 0.5. The marker genes of each cluster were identified using the “FindAllMarkers” function in Seurat with screening criteria $p_{\text{adj}} < 0.05$, $\log_2\text{fold change} > 0.5$, and minimum percentage of 0.25. For subclustering, cells belonging to FC, LC, and PC populations (primary clusters 1, 2, 3, 6, and 10) were extracted, and the raw counts were read into Seurat to create a new Seurat object. The next subclustering was performed as primary clustering with appropriate parameters: $\text{dims} = 15$, $\text{n.neighbors} = 40$, $\text{resolution} = 1.0$, and $\text{min.dist} = 0.01$. The DEGs between pistils and between stamens in different tissues were calculated using the “FindMarkers” function, and the GO analysis was performed by TBtools (Chen et al., 2020). The significance “ p_{adj} ” mentioned in this study represents the corrected p value using the Benjamini–Hochberg method.

Trajectory inference and pseudotime analysis

To construct the pseudotime differentiation trajectory of pistil cells, raw counts of cells belonging to subclusters 5, 6, 11, 12, and 13 were extracted for the Monocle2 (v.2.18.0) algorithm (Qiu et al., 2017). The genes with a mean expression value ≥ 0.1 and a dispersion empirical value larger than the dispersion fit value were defined as high-variant gene (HVGs) or whole-trajectory-dependent genes, and the cells were ordered along the trajectory using HVGs and visualized in a reduced dimensional space by the DDRTree algorithm in Monocle2. The branch-dependent genes were identified by Monocle’s BEAM function with q value $< 1e-4$. The whole-trajectory-dependent and branch-dependent genes were visualized by the “plot_pseudotime_heatmap” and “plot_genes_branched_heatmap” function, respectively. The clustered gene models were used for function annotations and GO analysis by TBtools (Chen et al., 2020).

scRNA-seq co-expression analysis

To reveal the co-expression correlations between genes, a weighted gene co-expression network (WGCN) was created by the WGCNA (v1.69) R package (Langfelder and Horvath, 2008) using pistil-related cells. To construct the WGCN with scale-free topology, different values of soft thresholding power β were assessed for the network topology analysis, and the value of 1 was selected. The Pearson correlation coefficient and the unsigned network options were used to measure the correlation between the expression levels of gene pairs. Further, we selected the top 400 positively and negatively co-expressed genes of *TS1*, *TS2*, *GT1*, *RA3*, *OPR7*, and *OPR8* to construct WGCNs, which were visualized by Cytoscape (Shannon et al., 2003). All the gene annotation information in our study was downloaded from the MaizeGDB database, which can be accessed at the following link: https://www.maizegdb.org/gene_center/gene#downloadall.

DATA AVAILABILITY

The data generated in this study have been deposited in the Gene Expression Omnibus database of the National Center for Biotechnology Information with accession number GEO: GSE247571 and also in the Genome Sequence Archive in the China National Genomics Data Center with accession number CRA016916.

SUPPLEMENTAL INFORMATION

Supplemental information is available at *Molecular Plant Online*.

FUNDING

This work was supported by the National Natural Science Foundation of China (32172026, U22A20460 to F.Y.), the Interdisciplinary Sciences Research Institute (2662021JC005 to F.Y.), and 111 Project Crop genomics and Molecular Breeding (B20051 to F.Y.).

AUTHOR CONTRIBUTIONS

F.Y. and Y.S. conceived and designed the project. Y.S., L.K., and W.Z. performed the experiments. L.D. and Y.S. analyzed data. Y.S., L.D., D.J., and F.Y. wrote the manuscript.

ACKNOWLEDGMENTS

We thank Professor Z. Yuan (Shanghai Jiao Tong University) for critical discussions. We thank C. Zhang and X. Lu for providing EMS mutant seeds. We thank Spatial FISH for scRNA-seq library construction, and the high-performance computing platform at the National Key Laboratory of Crop Genetic Improvement at Huazhong Agricultural University. No conflict of interest declared.

Received: December 7, 2023

Revised: May 23, 2024

Accepted: June 11, 2024

Published: June 13, 2024

REFERENCES

- Acosta, I.F., Laparra, H., Romero, S.P., Schmelz, E., Hamberg, M., Mottinger, J.P., Moreno, M.A., and Dellaporta, S.L. (2009). *tasselseed1* is a lipoxygenase affecting jasmonic acid signaling in sex determination of maize. *Science* **323**:262–265.
- Ambrose, B.A., Lerner, D.R., Ciceri, P., Padilla, C.M., Yanofsky, M.F., and Schmidt, R.J. (2000). Molecular and genetic analyses of the *silky1* gene reveal conservation in floral organ specification between eudicots and monocots. *Mol. Cell* **5**:569–579.
- Bartlett, M.E., Williams, S.K., Taylor, Z., DeBlasio, S., Goldshmidt, A., Hall, D.H., Schmidt, R.J., Jackson, D.P., and Whipple, C.J. (2015). The maize PI/GLO ortholog *Zmm16/sterile tassel silky ear1* interacts with the zygomorphy and sex determination pathways in flower development. *Plant Cell* **27**:3081–3098.
- Becht, E., McInnes, L., Healy, J., Dutertre, C.-A., Kwok, I.W.H., Ng, L.G., Ginhoux, F., and Newell, E.W. (2019). Dimensionality reduction for visualizing single-cell data using UMAP. *Nat. Biotechnol.* **37**:38–44.
- Bensen, R.J., Johal, G.S., Crane, V.C., Tossberg, J.T., Schnable, P.S., Meeley, R.B., and Briggs, S.P. (1995). Cloning and characterization of the maize *An1* gene. *Plant Cell* **7**:75–84.
- Bernacki, M.J., Rusaczonok, A., Czarnocka, W., and Karpinski, S. (2021). Salicylic acid accumulation controlled by *LSD1* is essential in triggering cell death in response to abiotic stress. *Cells* **10**:962.
- Best, N.B., Hartwig, T., Budka, J., Fujioka, S., Johal, G., Schulz, B., and Dilkes, B.P. (2016). *nana plant2* encodes a maize ortholog of the *Arabidopsis* brassinosteroid biosynthesis gene *DWARF1*, identifying developmental interactions between brassinosteroids and gibberellins. *Plant Physiol.* **171**:2633–2647.
- Bolger, A.M., Lohse, M., and Usadel, B. (2014). Trimmomatic: a flexible trimmer for Illumina sequence data. *Bioinformatics* **30**:2114–2120.
- Bortiri, E., Chuck, G., Vollbrecht, E., Rocheford, T., Martienssen, R., and Hake, S. (2006). *ramosa2* encodes a LATERAL ORGAN BOUNDARY domain protein that determines the fate of stem cells in branch meristems of maize. *Plant Cell* **18**:574–585.
- Brodersen, P., Malinovsky, F.G., Hématy, K., Newman, M.-A., and Mundy, J. (2005). The role of salicylic acid in the induction of cell death in *Arabidopsis acd11*. *Plant Physiol.* **138**:1037–1045.

- Calderon-Urrea, A., and Dellaporta, S.L. (1999). Cell death and cell protection genes determine the fate of pistils in maize. *Development* **126**:435–441.
- Char, S.N., Neelakandan, A.K., Nahampun, H., Frame, B., Main, M., Spalding, M.H., Becraft, P.W., Meyers, B.C., Walbot, V., Wang, K., and Yang, B. (2017). An Agrobacterium-delivered CRISPR/Cas9 system for high-frequency targeted mutagenesis in maize. *Plant Biotechnol. J.* **15**:257–268.
- Chen, Z., and Gallavotti, A. (2021). Improving architectural traits of maize inflorescences. *Mol. Breed.* **41**:21.
- Chen, Y., Hou, M., Liu, L., Wu, S., Shen, Y., Ishiyama, K., Kobayashi, M., McCarty, D.R., and Tan, B.-C. (2014). The maize *DWARF1* encodes a gibberellin 3-oxidase and is dual localized to the nucleus and cytosol. *Plant Physiol.* **166**:2028–2039.
- Chen, C., Chen, H., Zhang, Y., Thomas, H.R., Frank, M.H., He, Y., and Xia, R. (2020). TBtools: an integrative toolkit developed for interactive analyses of big biological data. *Mol. Plant* **13**:1194–1202.
- Choudhury, F.K., Rivero, R.M., Blumwald, E., and Mittler, R. (2017). Reactive oxygen species, abiotic stress and stress combination. *Plant J.* **90**:856–867.
- Chuck, G., Muszynski, M., Kellogg, E., Hake, S., and Schmidt, R.J. (2002). The control of spikelet meristem identity by the *branched silkleless1* gene in maize. *Science* **298**:1238–1241.
- Chuck, G., Meeley, R., Irish, E., Sakai, H., and Hake, S. (2007). The maize *tasselseed4* microRNA controls sex determination and meristem cell fate by targeting *Tasselseed6/indeterminate spikelet1*. *Nat. Genet.* **39**:1517–1521.
- Coll, N.S., Vercammen, D., Smidler, A., Clover, C., Van Breusegem, F., Dangl, J.L., and Eppe, P. (2010). *Arabidopsis* type I metacaspases control cell death. *Science* **330**:1393–1397.
- Coll, N.S., Smidler, A., Puigvert, M., Popa, C., Valls, M., and Dangl, J.L. (2014). The plant metacaspase AtMC1 in pathogen-triggered programmed cell death and aging: functional linkage with autophagy. *Cell Death Differ.* **21**:1399–1408.
- Cui, F., Brosché, M., Sipari, N., Tang, S., and Overmyer, K. (2013). Regulation of ABA dependent wound induced spreading cell death by MYB108. *New Phytol.* **200**:634–640.
- DeLong, A., Calderon-Urrea, A., and Dellaporta, S.L. (1993). Sex determination gene *TASSELSEED2* of maize encodes a short-chain alcohol dehydrogenase required for stage-specific floral organ abortion. *Cell* **74**:757–768.
- Dobin, A., Davis, C.A., Schlesinger, F., Drenkow, J., Zaleski, C., Jha, S., Batut, P., Chaisson, M., and Gingeras, T.R. (2013). STAR: ultrafast universal RNA-seq aligner. *Bioinformatics* **29**:15–21.
- Doll, N.M., Van Hautegeem, T., Schilling, N., De Rycke, R., De Winter, F., Fendrych, M., and Nowack, M.K. (2023). Endosperm cell death promoted by *NAC* transcription factors facilitates embryo invasion in *Arabidopsis*. *Curr. Biol.* **33**:3785–3795.e6.
- Du, Y., Wu, B., Xing, Y., and Zhang, Z. (2022). Conservation and divergence: Regulatory networks underlying reproductive branching in rice and maize. *J. Adv. Res.* **41**:179–190.
- Durian, G., Sedaghatmehr, M., Matallana-Ramirez, L.P., Schilling, S.M., Schaepe, S., Guerra, T., Herde, M., Witte, C.-P., Mueller-Roeber, B., Schulze, W.X., et al. (2020). Calcium-dependent protein kinase CPK1 controls cell death by in vivo phosphorylation of senescence master regulator ORE1. *Plant Cell* **32**:1610–1625.
- Fletcher, J.C. (2018). The CLV-WUS Stem Cell Signaling Pathway: A roadmap to crop yield optimization. *Plants* **7**:E87.
- Gallavotti, A., Zhao, Q., Kyozuka, J., Meeley, R.B., Ritter, M.K., Doebley, J.F., Pè, M.E., and Schmidt, R.J. (2004). The role of *barren stalk1* in the architecture of maize. *Nature* **432**:630–635.
- Gallavotti, A., Barazesh, S., Malcomber, S., Hall, D., Jackson, D., Schmidt, R.J., and McSteen, P. (2008). *sparse inflorescence1* encodes a monocot-specific *YUCCA*-like gene required for vegetative and reproductive development in maize. *Proc. Natl. Acad. Sci. USA* **105**:15196–15201.
- Galli, M., Liu, Q., Moss, B.L., Malcomber, S., Li, W., Gaines, C., Federici, S., Roshkovan, J., Meeley, R., Nemhauser, J.L., and Gallavotti, A. (2015). Auxin signaling modules regulate maize inflorescence architecture. *Proc. Natl. Acad. Sci. USA* **112**:13372–13377.
- Hao, Y., Hao, S., Andersen-Nissen, E., Mauck, W.M., Zheng, S., Butler, A., Lee, M.J., Wilk, A.J., Darby, C., Zager, M., et al. (2021). Integrated analysis of multimodal single-cell data. *Cell* **184**:3573–3587.e29.
- Hartwig, T., Chuck, G.S., Fujioka, S., Klempien, A., Weizbauer, R., Potluri, D.P.V., Choe, S., Johal, G.S., and Schulz, B. (2011). Brassinosteroid control of sex determination in maize. *Proc. Natl. Acad. Sci. USA* **108**:19814–19819.
- Hayward, A.P., Moreno, M.A., Howard, T.P., Hague, J., Nelson, K., Heffelfinger, C., Romero, S., Kausch, A.P., Glauser, G., Acosta, I.F., et al. (2016). Control of sexuality by the *sk1*-encoded UDP-glycosyltransferase of maize. *Sci. Adv.* **2**:e1600991.
- Heijmans, K., Morel, P., and Vandenbussche, M. (2012). *MADS-box* genes and floral development: the dark side. *J. Exp. Bot.* **63**:5397–5404.
- Huysmans, M., Buono, R.A., Skorzinski, N., Radio, M.C., De Winter, F., Parizot, B., Mertens, J., Karimi, M., Fendrych, M., and Nowack, M.K. (2018). *NAC* transcription factors *ANAC087* and *ANAC046* control distinct aspects of programmed cell death in the *Arabidopsis* columella and lateral root cap. *Plant Cell* **30**:2197–2213.
- Jackson, D., Veit, B., and Hake, S. (1994). Expression of maize *KNOTTED1* related homeobox genes in the shoot apical meristem predicts patterns of morphogenesis in the vegetative shoot. *Development* **120**:405–413.
- Je, B.I., Gruel, J., Lee, Y.K., Bommert, P., Arevalo, E.D., Eveland, A.L., Wu, Q., Goldshmidt, A., Meeley, R., Bartlett, M., et al. (2016). Signaling from maize organ primordia via *FASCIATED EAR3* regulates stem cell proliferation and yield traits. *Nat. Genet.* **48**:785–791.
- Ji, L., Liu, X., Yan, J., Wang, W., Yumul, R.E., Kim, Y.J., Dinh, T.T., Liu, J., Cui, X., Zheng, B., et al. (2011). *ARGONAUTE10* and *ARGONAUTE1* regulate the termination of floral stem cells through two microRNAs in *Arabidopsis*. *PLoS Genet.* **7**:e1001358.
- Kamoun, S., van West, P., Vleeshouwers, V.G.A.A., de Groot, K.E., and Govers, F. (1998). Resistance of *Nicotiana benthamiana* to *Phytophthora infestans* is mediated by the recognition of the elicitor protein INF1. *Plant Cell* **10**:1413–1425.
- Keegstra, K. (2010). Plant Cell Walls. *Plant Physiol.* **154**:483–486.
- Kim, J.C., Laparra, H., Calderón-Urrea, A., Mottinger, J.P., Moreno, M.A., and Dellaporta, S.L. (2007). Cell cycle arrest of stamen initials in maize sex determination. *Genetics* **177**:2547–2551.
- Kim, D., Paggi, J.M., Park, C., Bennett, C., and Salzberg, S.L. (2019). Graph-based genome alignment and genotyping with HISAT2 and HISAT-genotype. *Nat. Biotechnol.* **37**:907–915.
- Klein, H., Gallagher, J., Demesa-Arevalo, E., Abraham-Juárez, M.J., Heeney, M., Feil, R., Lunn, J.E., Xiao, Y., Chuck, G., Whipple, C., et al. (2022). Recruitment of an ancient branching program to suppress carpel development in maize flowers. *Proc. Natl. Acad. Sci. USA* **119**:e2115871119.
- Kobayashi, M., Ohura, I., Kawakita, K., Yokota, N., Fujiwara, M., Shimamoto, K., Doke, N., and Yoshioka, H. (2007). Calcium-dependent protein kinases regulate the production of reactive oxygen species by potato NADPH oxidase. *Plant Cell* **19**:1065–1080.

- Langfelder, P., and Horvath, S. (2008). WGCNA: an R package for weighted correlation network analysis. *BMC Bioinf.* **9**:559.
- Laudencia-Chinguanco, D., and Hake, S. (2002). The *indeterminate floral apex1* gene regulates meristem determinacy and identity in the maize inflorescence. *Development* **129**:2629–2638.
- Lawit, S.J., Wych, H.M., Xu, D., Kundu, S., and Tomes, D.T. (2010). Maize DELLA proteins dwarf plant8 and dwarf plant9 as modulators of plant development. *Plant Cell Physiol.* **51**:1854–1868.
- Lee, M.-H., Jeon, H.S., Kim, H.G., and Park, O.K. (2017). An *Arabidopsis* NAC transcription factor *NAC4* promotes pathogen-induced cell death under negative regulation by *microRNA164*. *New Phytol.* **214**:343–360.
- Li, Q., and Liu, B. (2017). Genetic regulation of maize flower development and sex determination. *Planta* **245**:1–14.
- Li, H., Handsaker, B., Wysoker, A., Fennell, T., Ruan, J., Homer, N., Marth, G., Abecasis, G., and Durbin, R.; 1000 Genome Project Data Processing Subgroup (2009). The sequence alignment/map format and SAMtools. *Bioinformatics* **25**:2078–2079.
- Li, C., Zhang, S., Yan, X., Cheng, P., and Yu, H. (2023). Single-nucleus sequencing deciphers developmental trajectories in rice pistils. *Dev. Cell* **58**:694–708.e4.
- Liang, L., Zhou, L., Tang, Y., Li, N., Song, T., Shao, W., Zhang, Z., Cai, P., Feng, F., Ma, Y., et al. (2019). A sequence-indexed mutator insertional library for maize functional genomics study. *Plant Physiol.* **181**:1404–1414.
- Liao, Y., Smyth, G.K., and Shi, W. (2014). featureCounts: an efficient general purpose program for assigning sequence reads to genomic features. *Bioinformatics* **30**:923–930.
- Liu, H., Ding, Y., Zhou, Y., Jin, W., Xie, K., and Chen, L.-L. (2017). CRISPR-P 2.0: an improved CRISPR-Cas9 tool for genome editing in plants. *Mol. Plant* **10**:530–532.
- Liu, L., Gallagher, J., Arevalo, E.D., Chen, R., Skopelitis, T., Wu, Q., Bartlett, M., and Jackson, D. (2021). Enhancing grain-yield-related traits by CRISPR-Cas9 promoter editing of maize *CLE* genes. *Nat. Plants* **7**:287–294.
- Liu, Z., Kong, X., Long, Y., Liu, S., Zhang, H., Jia, J., Cui, W., Zhang, Z., Song, X., Qiu, L., et al. (2023). Integrated single-nucleus and spatial transcriptomics captures transitional states in soybean nodule maturation. *Nat. Plants* **9**:515–524.
- Love, M.I., Huber, W., and Anders, S. (2014). Moderated estimation of fold change and dispersion for RNA-seq data with DESeq2. *Genome Biol.* **15**:550.
- Lu, X., Liu, J., Ren, W., Yang, Q., Chai, Z., Chen, R., Wang, L., Zhao, J., Lang, Z., Wang, H., et al. (2018). Gene-indexed mutations in maize. *Mol. Plant* **11**:496–504.
- Lunde, C., Kimberlin, A., Leiboff, S., Koo, A.J., and Hake, S. (2019). *Tasselseed5* overexpresses a wound-inducible enzyme, *ZmCYP94B1*, that affects jasmonate catabolism, sex determination, and plant architecture in maize. *Commun. Biol.* **2**:114.
- Makarevitch, I., Thompson, A., Muehlbauer, G.J., and Springer, N.M. (2012). *Brd1* gene in maize encodes a brassinosteroid C-6 oxidase. *PLoS One* **7**:e30798.
- McGinnis, C.S., Murrow, L.M., and Gartner, Z.J. (2019). DoubletFinder: doublet detection in single-cell RNA sequencing data using artificial nearest neighbors. *Cell Syst.* **8**:329–337.e4.
- McSteen, P., Malcomber, S., Skirpan, A., Lunde, C., Wu, X., Kellogg, E., and Hake, S. (2007). *barren inflorescence2* encodes a co-ortholog of the PINOID serine/threonine kinase and is required for organogenesis during inflorescence and vegetative development in maize. *Plant Physiol.* **144**:1000–1011.
- Nickerson, N.H. (1959). Sustained treatment with gibberellic acid of five different kinds of maize. *Ann. Mo. Bot. Gard.* **46**:19–37.
- Otero, S., Gildea, I., Roszak, P., Lu, Y., Di Vittori, V., Bourdon, M., Kalmbach, L., Blob, B., Heo, J.O., Peruzzo, F., et al. (2022). A root phloem pole cell atlas reveals common transcriptional states in protophloem-adjacent cells. *Nat. Plants* **8**:954–970.
- Phillips, K.A., Skirpan, A.L., Liu, X., Christensen, A., Slewinski, T.L., Hudson, C., Barazesh, S., Cohen, J.D., Malcomber, S., and McSteen, P. (2011). *vanishing tassel2* encodes a grass-specific tryptophan aminotransferase required for vegetative and reproductive development in maize. *Plant Cell* **23**:550–566.
- Qiu, X., Hill, A., Packer, J., Lin, D., Ma, Y.-A., and Trapnell, C. (2017). Single-cell mRNA quantification and differential analysis with Census. *Nat. Methods* **14**:309–315.
- Ramírez, F., Bhardwaj, V., Arrigoni, L., Lam, K.C., Grüning, B.A., Villaveces, J., Habermann, B., Akhtar, A., and Manke, T. (2018). High-resolution TADs reveal DNA sequences underlying genome organization in flies. *Nat. Commun.* **9**:1–15.
- Ren, D., Yang, H., and Zhang, S. (2002). Cell death mediated by MAPK is associated with hydrogen peroxide production in *Arabidopsis*. *J. Biol. Chem.* **277**:559–565.
- Salvesen, G.S., Hempel, A., and Coll, N.S. (2016). Protease signaling in animal and plant-regulated cell death. *FEBS J.* **283**:2577–2598.
- Satoh-Nagasawa, N., Nagasawa, N., Malcomber, S., Sakai, H., and Jackson, D. (2006). A trehalose metabolic enzyme controls inflorescence architecture in maize. *Nature* **441**:227–230.
- Satterlee, J.W., Strable, J., and Scanlon, M.J. (2020). Plant stem-cell organization and differentiation at single-cell resolution. *Proc. Natl. Acad. Sci. USA* **117**:33689–33699.
- Shannon, P., Markiel, A., Ozier, O., Baliga, N.S., Wang, J.T., Ramage, D., Amin, N., Schwikowski, B., and Ideker, T. (2003). Cytoscape: a software environment for integrated models of biomolecular interaction networks. *Genome Res.* **13**:2498–2504.
- Strable, J., and Vollbrecht, E. (2019). Maize *YABBY* genes *drooping leaf1* and *drooping leaf2* regulate floret development and floral meristem determinacy. *Development* **146**:dev171181.
- Stuart, T., Butler, A., Hoffman, P., Hafemeister, C., Papalexi, E., Mauck, W.M., Hao, Y., Stoeckius, M., Smibert, P., and Satija, R. (2019). Comprehensive integration of single-Cell data. *Cell* **177**:1888–1902.e21.
- Theißen, G., Strater, T., Fischer, A., and Saedler, H. (1995). Structural characterization, chromosomal localization and phylogenetic evaluation of two pairs of *AGAMOUS*-like *MADS-box* genes from maize. *Gene* **156**:155–166.
- Thompson, B.E., Bartling, L., Whipple, C., Hall, D.H., Sakai, H., Schmidt, R., and Hake, S. (2009). *bearded-ear* encodes a MADS box transcription factor critical for maize floral development. *Plant Cell* **21**:2578–2590.
- Valdivia, E.R., Herrera, M.T., Gianzo, C., Fidalgo, J., Revilla, G., Zarra, I., and Sampedro, J. (2013). Regulation of secondary wall synthesis and cell death by NAC transcription factors in the monocot *Brachypodium distachyon*. *J. Exp. Bot.* **64**:1333–1343.
- Van Opdenbosch, N., and Lamkanfi, M. (2019). Caspases in cell death, inflammation, and disease. *Immunity* **50**:1352–1364.
- Veit, B., Briggs, S.P., Schmidt, R.J., Yanofsky, M.F., and Hake, S. (1998). Regulation of leaf initiation by the *terminal ear 1* gene of maize. *Nature* **393**:166–168.
- Vollbrecht, E., Springer, P.S., Goh, L., Buckler, E.S., and Martienssen, R. (2005). Architecture of floral branch systems in maize and related grasses. *Nature* **436**:1119–1126.
- Wang, F., Yu, Z., Zhang, M., Wang, M., Lu, X., Liu, X., Li, Y., Zhang, X., Tan, B.-C., Li, C., and Ding, Z. (2022). *ZmTE1* promotes plant height

- by regulating intercalary meristem formation and internode cell elongation in maize. *Plant Biotechnol. J.* **20**:526–537.
- Winkler, R.G., and Helentjaris, T.** (1995). The maize *Dwarf3* gene encodes a cytochrome P450-mediated early step in Gibberellin biosynthesis. *Plant Cell* **7**:1307–1317.
- Wrzaczek, M., Vainonen, J.P., Stael, S., Tsiatsiani, L., Help-Rinta-Rahko, H., Gauthier, A., Kaufholdt, D., Bollhöner, B., Lamminmäki, A., Staes, A., et al.** (2015). GRIM REAPER peptide binds to receptor kinase PRK5 to trigger cell death in *Arabidopsis*. *EMBO J.* **34**:55–66.
- Xanthoudakis, S., and Nicholson, D.W.** (2000). Heat-shock proteins as death determinants. *Nat. Cell Biol.* **2**:E163–E165.
- Xu, X., Crow, M., Rice, B.R., Li, F., Harris, B., Liu, L., Demesa-Arevalo, E., Lu, Z., Wang, L., Fox, N., et al.** (2021). Single-cell RNA sequencing of developing maize ears facilitates functional analysis and trait candidate gene discovery. *Dev. Cell* **56**:557–568.e6.
- Yan, Y., Christensen, S., Isakeit, T., Engelberth, J., Meeley, R., Hayward, A., Emery, R.J.N., and Kolomiets, M.V.** (2012). Disruption of *OPR7* and *OPR8* reveals the versatile functions of jasmonic acid in maize development and defense. *Plant Cell* **24**:1420–1436.
- Yoda, H., Hiroi, Y., and Sano, H.** (2006). Polyamine oxidase is one of the key elements for oxidative burst to induce programmed cell death in tobacco cultured cells. *Plant Physiol.* **142**:193–206.
- Zhang, T.-Q., Xu, Z.-G., Shang, G.-D., and Wang, J.-W.** (2019). A Single-cell RNA sequencing profiles the developmental landscape of *Arabidopsis* root. *Mol. Plant* **12**:648–660.
- Zhang, T.-Q., Chen, Y., and Wang, J.-W.** (2021). A single-cell analysis of the *Arabidopsis* vegetative shoot apex. *Dev. Cell* **56**:1056–1074.e8.
- Zhang, L., He, C., Lai, Y., Wang, Y., Kang, L., Liu, A., Lan, C., Su, H., Gao, Y., Li, Z., et al.** (2023). Asymmetric gene expression and cell-type-specific regulatory networks in the root of bread wheat revealed by single-cell multiomics analysis. *Genome Biol.* **24**:65.
- Zhao, Z., Yang, S.-J., Yin, X.-X., Yan, X.-L., Hassan, B., Fan, J., Li, Y., and Wang, W.-M.** (2023). *ARGONAUTE 1*: a node coordinating plant disease resistance with growth and development. *Phytopathol. Res.* **5**:38.
- Zhu, X., Xu, Z., Wang, G., Cong, Y., Yu, L., Jia, R., Qin, Y., Zhang, G., Li, B., Yuan, D., et al.** (2023). Single-cell resolution analysis reveals the preparation for reprogramming the fate of stem cell niche in cotton lateral meristem. *Genome Biol.* **24**:194–231.
- Zong, J., Wang, L., Zhu, L., Bian, L., Zhang, B., Chen, X., Huang, G., Zhang, X., Fan, J., Cao, L., et al.** (2022). A rice single cell transcriptomic atlas defines the developmental trajectories of rice floret and inflorescence meristems. *New Phytol.* **234**:494–512.